Seismic assessment of existing steel frames with masonry infills

Luigi Di Sarno, Jing-Ren Wu

Department of Civil Engineering and Industrial Design, School of Engineering, University of Liverpool, L69 3GH, United Kingdom

Abstract

Many existing steel moment-resisting frames were constructed before the provisions of modern seismic codes; therefore, they are likely to exhibit high vulnerability to earthquakes due to their inadequate ductility design, hence low energy dissipation capacity. Public concern has been raised about the development of a reliable code-based framework for assessing existing structures, however, previous research has shown that the current European code EC8-3 may not be sufficient and requires urgent improvements. Particular attention should be paid to the contribution from infill walls in steel buildings, especially those made of masonry, and beam-column connections, as they play a significant role in the structural performance under earthquakes. To this end, an updated assessment procedure, which is an extension of the current procedure in EC8-3 but with several improvements to the non-linear analysis methods, is proposed in this paper and is applied to an existing steel building as a case study. The building is a three-storey steel moment-resisting frame located at Amatrice in Central Italy, which survived the recent 2016-2017 Central Italy earthquakes. Refined 3D models of the case study building, which account for the effects of infill walls and column panel zones, were implemented in a refined finite element platform. The effects of masonry infills on structural components, such as beams and columns, were investigated through non-linear analysis methods. The results emphasise the significance of including masonry infills in the numerical model for seismic assessment especially when an optimised retrofit solution is needed.

Keywords: standardised seismic assessment, existing steel frame, masonry infills, column panel zones.

1 Introduction

Numerous existing steel moment-resisting frames (MRFs) were constructed prior to the provision of modern seismic design codes [1, 2, 3, 4, 5]. These steel MRFs have shown high vulnerability to strong earthquakes due to lack of adequate seismic design and low energy dissipation capacity as a result of inadequate ductile detailing [3]. The recent 2016-2017 Central Italy earthquakes have emphasised the vital importance of providing a reliable framework to assess the seismic vulnerability of existing steel MRFs in order to avoid the collapse of existing structures and to allow the design of efficient retrofitting solutions. Several code-based procedures, such as the Eurocode 8-Part 3 (EC8-3) [6] and the American guidance ASCE41-17 [7], which are representatives of the latest generation of codes for the assessment of existing steel MRFs developed under the framework of Performance-Based Earthquake Engineering [8, 9, 10].

Previous studies [3, 11, 12, 13] have performed assessment and evaluations on the current provisions in EC8-3 and some issues have been raised with respect to the adequacy and reliability of the European codified assessment procedure. Amongst others, Araújo and Castro [11] performed a comparative study of the European and American procedures and highlighted some limitations in the current EC8-3, such as the lack of safety verification criteria for linear analysis method and inconsistencies in seismic demands obtained from different analysis methods. In addition, it has been pointed out that the compliance criteria for assessing steel beams and columns reported in EC8-3 is found to be identical to the relevant acceptance criteria in the old version American code ASCE41-06 [14], which have been improved in its successors [7, 15]. Furthermore, the EC8-3 requires safety checks to be carried out on every single element, which can be very time-consuming for large spatial models, and the capacity for a certain limit state simply takes the onset of the first element

that fails the limit state, which is on the safe side but will lead to higher cost for retrofit since any possible redundancy of the structure is neglected [13].

A major issue in the code-based assessment procedure of existing buildings is related to the numerical modelling of the case study building, particularly the modelling of non-structural components. For the case of steel MRFs, the easiest and most common way is to build a model of bare frame, with beam-column connections simplified as single nodes and storey mass lumped at the centre of mass (CM) for spatial models. However, given the complex behaviour of the interactions between structural and non-structural components [16, 17, 18], models that neglected the effects of infills and column panel zones are therefore not adequate for a holistic assessment of existing buildings. The presence of masonry infills will increase the lateral strength and stiffness of steel MRFs but will also cause concentrated damage to column ends due to its strut action [3, 53]. It is reported in [53] that for a seismically-designed steel frame, the presence of infills may lead to more than 50% reduction in the fundamental translational period, and the reduction can be even higher for shorter buildings. Considering the fact that non-seismically-designed steel frames are more flexible than modern buildings, the reduction in fundamental period is likely to be greater than 50%. The importance of infills has been recognised by the European code [19], as in the q-factor approach for design of new buildings, the value of q for infilled steel frames is half of that for bare frames, i.e. 2 for infilled frames and 4 for bare frames [19]. However, there is still no reflection in the EC8-3 for assessing existing buildings. To account for the presence of masonry infills in the modelling of MRFs, an effective approach has been developed, which makes use of a single strut in each diagonal direction to represent the infill wall panel [20, 21, 22, 41]. The struts normally have the same thickness as the infill walls and adopt an equivalent width determined based on the properties of infills and the confining frame [22]. The single strut model is able to provide adequate efficiency and accuracy in the assessment

of structural response at the global level, despite some sacrifice of the local behaviour of the structures. Apart from the contribution of infill walls, previous studies show that column panel zones also play an important role in steel MRFs, especially when subjected to combined gravity and horizontal loads [2, 23, 24]. In such cases, large unbalanced bending moment may occur at beam-column connections, causing complicated stress distribution within the column panel zone and affecting the seismic performance of steel MRFs. Some analytical models of column panel zone have been developed, which utilise either a diagonal spring [24] or a rotational spring [2] to capture the shear behaviour of panel zones.

The incorporation of modelling of infill walls and column panel zones can be challenging for the current procedure in EC8-3 due to its limited applicability to assessing infilled steel MRFs. This is illustrated mainly in two aspects. On one hand, the current EC8-3 lacks acceptance criteria for evaluating infills and column panel zones, and the use of chord rotation limits only is believed to be inadequate considering the contribution from infills and panel zones. The American code has already recognised this inadequacy and provides relevant criteria for masonry infills and column panel zones [7, 15]. On the other hand, the method adopted in the non-linear static analysis (NSA) for estimating target displacements is the conventional N2 method [25], which is not suitable in the case of assessing infilled steel MRFs as the presence of infills may significantly affect the response of structures and lead to a completely different capacity curve [26, 28].

Apart from the above mentioned challenges for the current EC8-3, some other issues are also identified in literature, mainly related to non-linear dynamic analysis (NDA). For example, the current earthquake record selection procedure in EC8 framework, which does not put any restrictions on earthquake characteristic parameters, is believed to be rather simplified and may lead to erroneous results in practical design and assessments [29, 30]. Also, the EC8-3 address the probability issue of seismic response in a deterministic way, however, it does not

clearly state the variability of using different groups of earthquakes, and this 'record-to-record variability' requires further justification [31]. Furthermore, the current EC8-3 does not provide specific guidance on how to evaluate the damage accumulation of structures under earthquake sequences especially in the context of dynamic analysis where the influence of aftershocks is often neglected [32, 33, 34].

2 Aims of the paper

The limitations of the current assessment framework in EC8-3 emphasise the necessity of developing improved analysis methods for the seismic assessment of existing steel MRFs, which are able to account for the effects of non-structural components. It is also important to understand the effects of masonry infills on the behaviour of steel beams and columns such that an optimised retrofit solution can be determined. This paper will be primarily aimed at proposing a NSA procedure for assessing steel MRFs with infills and showing the feasibility of its application on a case study building. The assessment will be carried out using the proposed NSA approach implemented on 3D finite element (FE) models of the case study building with and without masonry infills to estimate the seismic demands and to perform safety verifications. The results will be compared to those obtained from code-based NDA methods to assess the reliability of the proposed method. The effects of infill walls on the overall structural performance of the case study steel MRF will also be examined during the assessment procedure, in particular their effects on the beams and columns.

3 Assessment of steel buildings according to EC8-3

EC8-3 requires the performance of existing buildings to be checked at three limit states, namely Damage Limitation (DL), Significant Damage (SD) and Near Collapse (NC) limit state. The return periods ascribe to the three limit states are 225, 475 and 2475 years for DL, SD and NC LS respectively, associated with probabilities of exceedance of 20, 10 and 2% in

50 years. This is different from the checks for new buildings in Eurocode 8-Part 1 (EC8-1) [19], which contains only two limit states as summarised in Table 1. By comparing with the definition of limit states in EC8-1, it is found that the SD limit state in EC8-3 has the same performance requirement as the ultimate limit state in EC8-1 in terms of their return period and probability of exceedance, though the former represents an economically repairable condition of existing buildings while the latter concerns about the overall safety of new structures. The NC limit state, which is a superior limit state to the SD limit state in EC8-3, requires little redundancy of damaged structures by definition and therefore is closer to the real collapse of an existing building. The definition of NC limit state reveals the fundamental difference between EC8-1 and EC8-3, where the former is aimed at design of modern buildings and tends to require more redundancy to be at the safe side, while the latter focuses more on the real condition of existing buildings in order to obtain optimised retrofit solutions. Since this study is based on nonlinear methods, the linear procedure will not be introduced and discussed hereafter.

	EC8-3			EC8-1	
	DL	SD	NC	DL	Ultimate
Return Period (years)	225	475	2475	95	475
$P_{exceedance}$	20% in 50 yrs	10% in 50 yrs	2% in 50 yrs	10% in 10 yrs	10% in 50 yrs

Table 1. Summary of return period and associated probability of exceedance of limit states defined in EC8-3 and EC8-1.

Apart from the performance requirements, EC8-3 also defines three knowledge levels (KL) to account for the potential lack of information of the geometry, detailing and materials of existing buildings: limited knowledge (KL1), normal knowledge (KL2) and full knowledge (KL3). The level of knowledge achieved determines the analysis methods that are allowed in the assessment and the value of confidence factor (CF) that is used to reduce the mean value

147 of material strength in the calculation of capacity. Linear analysis methods are allowed for all
148 three KLs while non-linear approaches are only allowed for KL2 and KL3. The proposed
149 values of CF are 1.35, 1.20 and 1.00 for KL1, KL2 and KL3, respectively.

150 For estimating the seismic demands, EC8-3 allows both linear and non-linear analysis
151 methods to be utilised, however, the latter is more straightforward as the demands can be
152 directly obtained from the response of non-linear analysis methods. As it is well-known, the
153 assessment procedure proposed in EC8-3 is a displacement-based procedure and the seismic
154 demand is represented through the target displacement, which is normally the lateral
155 displacement of the control node. A common choice of the control node is the CM at the top
156 floor. NSA, also known as pushover analysis, is easier to be performed than the cumbersome
157 and time-consuming NDA, allowing pushover analysis the potential to become the principle
158 analysis method in EC8-3 [24, 51]. According to EC8-3, two conventional lateral load
159 patterns, namely a 'uniform' pattern and a 'modal' pattern, shall be applied in the two
160 horizontal principle directions when a spatial model is used. The implementation of pushover
161 analyses also requires two issues to be addressed, which are the effects of higher modes and
162 torsion. To account for the contribution from higher modes, EC8-3 recommends the use of an
163 updated version of pushover analysis, but it does not explicitly refer to a specific version of
164 updated pushover approach to be used, although there are several adaptive pushover methods
165 developed in literature [35, 36, 37]. Besides, when the storey mass is lumped at the CM of
166 each storey and the lateral loads are assigned only to the CM, pushover analysis may
167 underestimate the lateral drift due to the torsional effects caused by irregular floor plan or
168 elevation. Therefore, to account for the torsional effects, an amplification factor obtained
169 from elastic modal analysis shall be applied to the target displacement of control node in
170 order to obtain the displacements at other nodes. Finally, the seismic demands are determined
171 using the conventional version of N2 method, which turns the structures into an equivalent

SDOF system and makes use of the target response spectrum in acceleration-displacement form [24]. The implementation of NDA is more straightforward compared to the pushover analysis. EC8-3 requires at least three ground motion records to be used, whose mean response spectrum achieves compatibility with the target spectrum, i.e. the mean spectrum should not be less than 90% of the target spectrum within the range $[0.2T_1, 2T_1]$, where T_1 is the fundamental period of the structure. If less than seven records are used, the maximum response shall be taken as the demand; otherwise the demand shall take the average response from all dynamic analyses. EC8-3 also requires that the two horizontal components of ground motion records shall be applied simultaneously to the spatial model.

The final stage of assessing existing buildings is the safety verification. For ductile components in SMRFs, the EC8-3 requires safety checks to be carried out by comparing the rotation demand at the end of beams and columns with their associated rotational capacities. The criteria are summarised in Table 2, on the condition that the dimensionless axial load ν of a member is not larger than 0.3, where the inelastic chord rotation capacities are simply a multiple of the chord rotation at yielding θ_y. However, despite that EC8-3 provides semi-empirical equations for estimating yield rotation for RC structures, there is no guidance on the calculation of yield rotation of steel beams and columns. There is no limit provided for higher value of dimensionless axial load ν, either. Apart from the chord rotation capacity limit, other limits based on axial deformation capacity of braces are also proposed in EC8-3 but are generally not used in the case of SMRFs.

	Limit state		
Class of cross section	DL	SD	NC
Class 1	1.0 θ_y	6.0 θ_y	8.0 θ_y
Class 2	0.25 θ_y	2.0 θ_y	3.0 θ_y

Table 2. Plastic rotation capacity at the end of beams and columns proposed in EC8-3.

4 Proposed methodology for assessing steel MRFs with masonry infills

To address the issues stated in the introductory sections, an improved NSA procedure designed to assess steel MRFs with modelling of different components is proposed in this paper, as introduced in Figure 1, which is based on the current procedure in EC8-3.

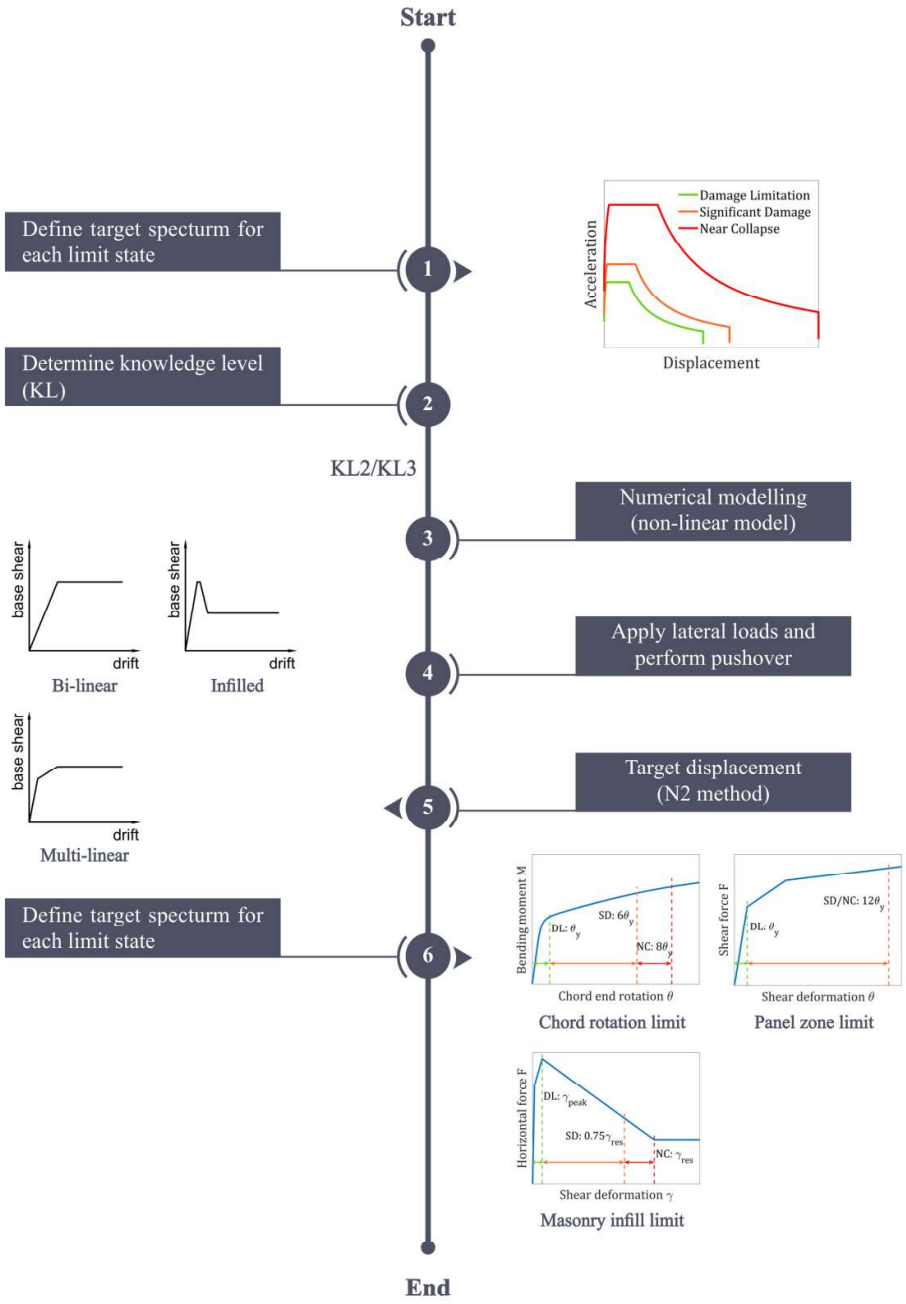

Figure 1. The proposed non-linear static analysis method for assessing steel MRFs with different components.

As shown in Figure 1, Step 1 to 3 follows the existing procedure in EC8-3. It should be noted that according to EC8-3 non-linear assessment is only permitted when KL2 or KL3 is achieved. Then at Step 4, at least the two conventional lateral load patterns should be applied, i.e. the 'modal' and 'uniform' pattern, as mentioned the previous section. Meanwhile, it is recommended that lateral loads should be applied to each node considering their assigned masses and associated displacement shapes, particularly in the case of spatial mode with irregular layout or elevation, in which cases the torsional effects are inherently accounted for.

Step 5 is to determine the target displacement for each limit state. A major difference here from the EC8-3 is that a modified N2 method developed by Dolšek and Fajfar [27, 28] for infilled frames is adopted in addition to the conventional N2 method for bare frames [25]. In any other cases when neither of the two N2 methods is appropriate, a multi-linear idealisation of capacity curves is proposed, whose effective elastic stiffness is determined following the rule suggested in [10] that the elastic segment of the multi-linear curve intersects the capacity curve at 60% of the idealised yield force and the total deformation energy should be approximately the same.

Step 6 is the safety verification, which is the final stage of assessing existing buildings. At this step, the proposed procedure involves additional criteria for assessing column panel zones and masonry infills, as a supplement to the chord rotation criteria in EC8-3. Those additional criteria follow the concept of displacement-based assessment, thus are all related to deformation parameters of components. For example, the performance of masonry infills are assessed based on lateral drift criteria, i.e. shear deformation under horizontal load, which are modified based on the criteria in the American code ASCE41-17 [7] for infilled frames with relatively low column shear strength, considering the performance requirements for different limit states in EC8-3. The criteria for column panel zones are also an adaptation from the American code [7], which are based on the shear distortion of column panel zones.

5 Application of the methodology: a case study

5.1 Case study building

The selected case study building is a three-storey steel MRF located in Amatrice, Italy, which was constructed decades ago, prior to the provision of modern seismic design code. The building was reported to survive the 2016-2017 Amatrice earthquakes and a site investigation of its damage condition was conducted in September, 2016 [3] after the first earthquake sequence took place in Amatrice (See Figure 3). Damage was found to be concentrated on lower floors of the building. Yielding was observed in columns, particularly at beam-column connections and masonry infills were significantly damaged with observed failure of finishes, but without out-of-plane collapse. The village is classified to be on type B ground in EC8 and in the region that has a reference ground acceleration of 0.25g with 10% probabilities of exceedance in 50 years, according to the seismic hazard zonation in Italy [50]. The design ground acceleration a_g is then taken as 0.20, 0.25 and 0.43g for DL, SD and NC limit state, respectively.

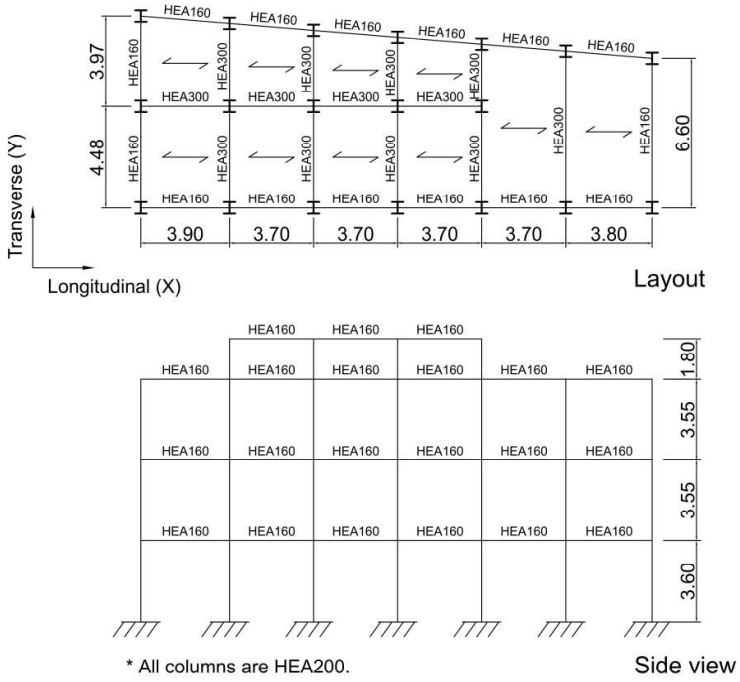

Figure 2. Schematic layout and side view of the case study steel frame (unit: m).

Figure 3. Surveyed damage of the case study building after the 2016-2017 earthquake sequence (significant damage on infills and yielding at beam-column connections).

The building is trapezoidal in its plan, which is 6.6 and 8.5m in width and 22.5m in length. The storey height is around 3.6m, adding up to a total height of 12.5m, which also includes a 1.8m-high roof floor. Figure 2 summarises the basic geometry of the case study building, and Figure 3 contains some photos of the building showing the damage detected during earthquake survey. In the rest of the paper, the longitudinal and transverse direction of the building are denoted as X and Y direction, respectively. The cross-sections of external and internal beams are HEA160 and HEA300, respectively, and all columns are HEA200. All the cross-sections can be classified as Class 1 cross-section and the steel grade used in design is S235 (f_y=235MPa). The strong axis of columns is in the Y direction of the buildings and beams are connected to columns through full penetration welding. Besides, the infill walls contain two layers of perforated clay bricks with dimension 120×250×80mm, contributing to a total thickness of 160mm. Based on the information collected, the knowledge level in this

257 case is determined to be KL2 due to lack of tests of actual material properties onsite.
258 Consequently, both linear and non-linear analysis methods are allowed in this case and the
259 corresponding CF takes the value of 1.2 as suggested by EC8-3.

260 **5.2 Structural modelling**

261 A total of six three-dimensional FE model of the case study building, were developed in
262 OpenSees [38] to investigate the contribution of different components and the influence of
263 the modelling assumptions on the seismic behaviour of the case study building. A summary
264 of the models investigated is reported in Table 3. In all models the building is considered to
265 be fixed at the base, and beams and columns are modelled using nonlinear element with fibre
266 section, whose behaviour is represented by the Giuffré-Menegotto-Pinto constitutive law with
267 appropriate parameters to account for the strength degradation [39, 40]. In principle, mean
268 material property obtained from onsite tests should be used in the assessment according to
269 EC8-3, however, due to the lack of such information, some assumptions have to be made
270 with respect to the material properties used in this paper. The mean yield strength of steel
271 used in the assessment is considered to be 215MPa instead of 235MPa, assuming a standard
272 deviation of 15MPa and also a CF of 1.2. The Young's modulus is 210GPa and the strain
273 hardening ratio is 0.02. For the masonry infill walls, the compressive strength of bricks and
274 mortar are considered to be 10 and 5MPa, respectively.

275 As indicated in Table 3, two different types of simplified modelling of the rigid slab are
276 considered: the slab type A refers to the use of rigid diaphragm constraint while the slab type
277 B refers to the use of rigid diagonal struts, where each corner of the slab is connected to the
278 opposite corner diagonally through horizontal rigid elements. This comparison is aimed at
279 verifying the equivalency of the two types of modelling approaches in terms their effects on
280 the modal properties of the structure. This also helps gain confidence in using type B slab as
281 a replacement of conventional rigid diaphragm constraints due to the fact that the

combination of rigid diaphragm constraints and modelling of column panel zones requires the centre node of each panel zone to be the master node of the other nodes in that panel zone and at the same time to be a slave node in the rigid diaphragm constraint, which is not allowed by OpenSees [38].

Model	Slab		Infills	Panel Zone
	Rigid diaphragm constraint	Rigid diagonal struts		
1	√			
2		√		
3	√		√	
4		√	√	
5		√		√
6		√	√	√

Table 3. Summary of models with different components investigated.

The additional models investigate the influence of the masonry infill walls and the column panel zones. Model 3, 4 and 6 include the modelling of masonry infills through the single strut model [41, 42]. This model is adopted in this paper due to its great simplicity and acceptable accuracy. The behaviour of the masonry infills is represented by the multi-linear curve developed by Liberatore and Decanini [43], as shown in Figure 4. In Model 5 and 6, a simplified model of the beam-column connection panel zone developed by Gupta and Krawinkler [2] is also included. As shown in Figure 5a, the column panel zone is modelled by small rigid elements, where the shear distortion is controlled by a rotational spring characterised by the backbone curve in Figure 5b. It should be noted that the panel zones are only present in the direction where beams are connected to the flange of columns, In the other direction, a small offset from the top of bottom column to the centre of panel zone is

298 achieved to ensure the beam is connected to the centre of the panel zone. Detailed
299 information of the parameters defining backbone curves of infill walls and column panel are
300 summarised in Table 4.

Infills						
	F_{cr} (kN)	F_u (kN)	Strain			κ
			δ_{cr}	δ_u	δ_r	
Longitudinal	113	143	6.81e-05	3.45e-04	4.37e-03	0.35
Transverse	128	160	5.79e-05	2.96e-04	3.57e-03	0.35
	119	149	5.52e-05	2.82e-04	3.60e-03	0.35
	168	210	6.31e-05	3.22e-04	4.07e-03	0.35
Panel zone						
	V_y (kN)	γ_y (rad)	V_p (kN)	γ_p (rad)	α	
Perimeter	24	1.54e-03	32	6.16e-03	0.02	
Internal	42	1.54e-03	49	6.16e-03	0.02	

301 Table 4. Parameters defining the backbone curves of infill walls and column panel zones (see
302 Figure 4 and 5 for notation).

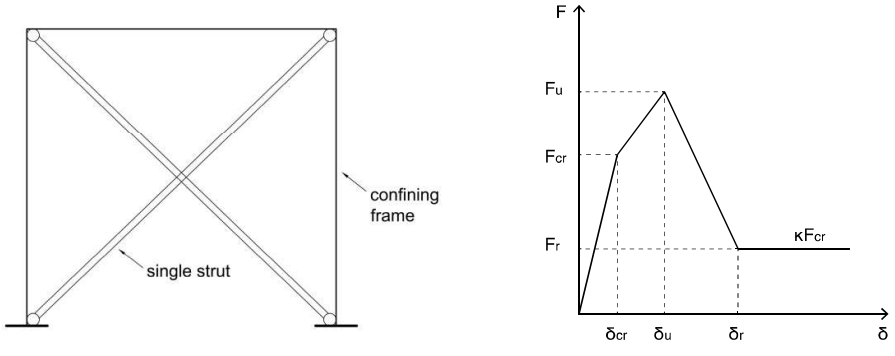

303
304 (a) (b)

305 Figure 4. Schematic view of the single strut model for masonry infill walls and illustration of
306 the multi-linear backbone curve.

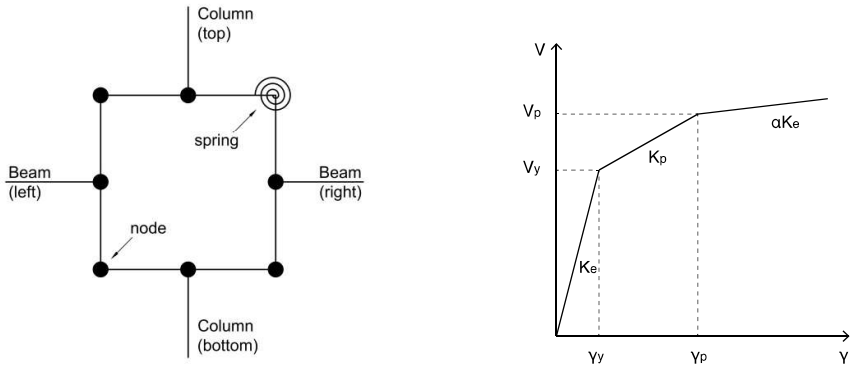

(a) (b)

Figure 5. Modelling of column panel zone and illustration of the tri-linear backbone curve.

5.3 Modal analysis response

Modal analyses were firstly performed on the FE models to investigate the effects of different modelling parameters, especially the masonry infills, on the modal properties of the case study structure. The corresponding period and modal mass of the first translational mode in the X and Y direction are summarised in Table 5.

The comparison of Modes 1 and 2, and Models 3 and 4 shows the limited influence of the modelling strategy used for slab, particularly in the X direction. This allows more confidence in the use of rigid diagonal struts as a replacement to the rigid diaphragm constraint in this study. When infills are incorporated into the model, the initial natural periods in the X and Y direction are significantly reduced to around 0.1 and 0.3sec, respectively, indicating the significant increase in lateral stiffness due to the presence of infill walls. However, the effects of infills on the modal mass are limited where only small variations are observed, which suggests that when the presence of infills are accounted for, the first mode still dominates the response of the structure in each direction. Since the column panel zones are only present in the Y direction of the structure, their major effects are reflected on the modal properties of the structure in the Y direction. The comparison of Models 2 and 5 shows that the inclusion of panel zones offers more flexibility in the Y direction, leading to approximately 10%

increase of the natural period and a slight drop of participating mass. It also increases the lateral stiffness in the X direction due to the reduced length of column elements, but the change is not significant.

In summary, when the infills and beam-column connection panel zones are accounted for in the model, different modal properties are obtained, so their effects on the seismic response of steel MRFs cannot be neglected. Therefore, the two most completed model, Models 5 and 6, will be assessed in the following sections of this paper.

Model	Slab type		Infills	Panel Zone	Fundamental translational mode			
					X		Y	
	A	B			Period (sec)	Mass (%)	Period (sec)	Mass (%)
1	√				1.86	89.13	1.17	84.11
2		√			1.86	89.13	1.17	84.04
3	√		√		0.10 (-95%)	87.59 (-2%)	0.27 (-77%)	89.03 (+6%)
4		√	√		0.11 (-94%)	87.02 (-2%)	0.31 (-74%)	87.77 (+4%)
5		√		√	1.75 (-6%)	90.05 (+1%)	1.27 (+9%)	81.68 (-3%)
6		√	√	√	0.11 (-94%)	87.12 (-2%)	0.32 (-73%)	87.26 (+4%)

Table 5. Summary of modal properties of models with different modelling parameters (increment or reduction in brackets are compared to Model 1).

5.4 Nonlinear static analysis

Pushover analyses were performed on the Models 5 and 6 described in Section 5.2, namely the 'bare frame' and the 'infilled frame' to investigate the performance of the case study structure with and without masonry infills based on the procedure proposed in Section 4. The lateral loads are applied all nodes considering their assigned masses and fundamental mode

shapes. It should be noted that since the bare and the infilled frame have different fundamental mode shapes, the lateral loads applied to the two models are different.

			Longitudinal (X)			Transverse (Y)		
			DL	SD	NC	DL	SD	NC
Bare frame	M	Pos	1.59	2.01	3.44	1.20	1.51	2.59
		Neg	1.58	2.00	3.43	1.21	1.54	2.63
	U	Pos	1.49	1.89	3.23	1.16	1.46	2.50
		Neg	1.49	1.89	3.23	1.16	1.46	2.54
Infilled frame	M	Pos	0.17	0.28	0.65	0.36	0.46	0.80
		Neg	0.13	0.23	0.56	0.38	0.48	0.84
	U	Pos	0.14	0.24	0.58	0.38	0.48	0.84
		Neg	0.08	0.17	0.46	0.40	0.51	0.89
$\frac{Demand_{Infilled}}{Demand_{bare}}$			11%	14%	19%	33%	33%	34%

Table 6. Target displacements in terms of lateral drift ratio (%) at top floor (M: modal pattern, U: uniform pattern, Pos: positive loading, Neg: negative loading).

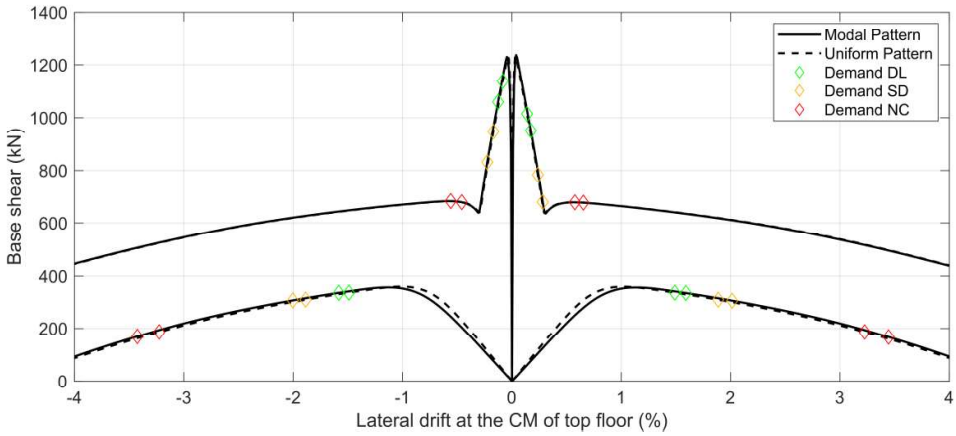

Figure 6. Capacity curves in the X direction.

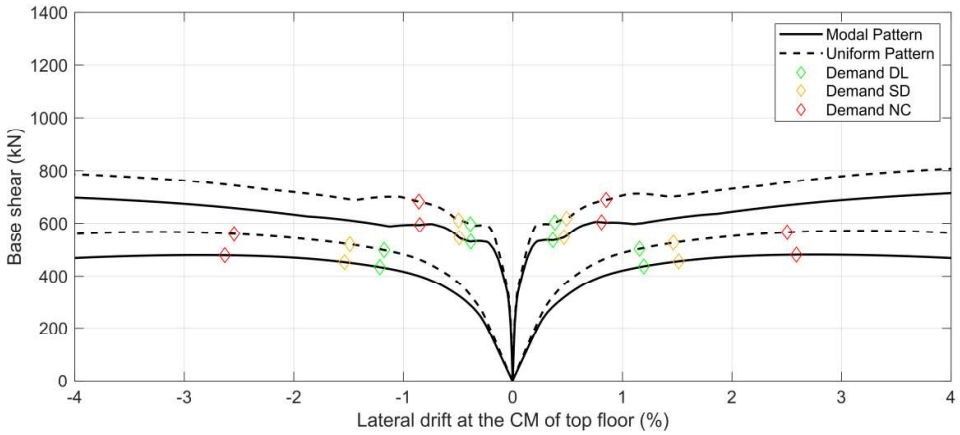

Figure 7. Capacity curves in the Y direction.

The capacity curves showing the evolution of base shear and lateral drift ratio at the CM of the top floor are presented in Figure 6 and Figure 7. It appears that the capacity curves in the positive and negative direction are generally symmetrical, and so, the inverse of lateral loading does not significantly change the structural performance. Also, the effects of infills are evident as they substantially increase the lateral stiffness and strength of the steel building, especially in the X direction. The ratio of maximum base shear to the total weight is 0.23 and 0.07 for the infilled and bare frame, respectively, in the X direction. The target displacements of the bare and infilled frame are summarised in Table 6, where the final values of target displacement for each limit state and direction take the largest value from all combination of load patterns and loading directions (positive or negative). The results indicate that the presence of masonry infills will effectively reduce the target displacement due to the increase in lateral stiffness of the structure. It is also noted that in the X direction, as shown in Figure 6, the target displacement of DL and SD limit state lie in the range with negative stiffness that is resulted from the failure of all infill walls on the ground floor, which emphasizes the importance of accounting for the effects of infills. Since the most critical target displacement of the infilled frame occurs in the case of positive modal pattern and negative uniform pattern in the X and Y direction, respectively, the results from the two loading cases will be discussed further in the rest of the paper.

By assessing the damage evolution in the structure, Figure 6 shows that in the X direction all the ground floor infills degrade at the peak point at around 0.04% drift and collapse at 0.3% drift, which is similar to the case of a RC infilled building in the study by Dolšek and Fajfar [26]. The 0.3% drift also marks the onset of yield of ground floor columns as the collapse of infill walls leads to substantial loss of lateral stiffness and strength and causes rapid redistribution of forces. In the Y direction, as shown in Figure 7, the major difference between the response of the bare and infilled frame are the two step-like stages in the capacity curve of the infilled frame, which are the result of the interaction between panel zones and infills in the transverse direction. The first step (0.2-0.45% drift) corresponds to the yield of ground floor column panel zones and the second step (0.45-1.45% drift) corresponds to the yield of column panel zones on the first floor.

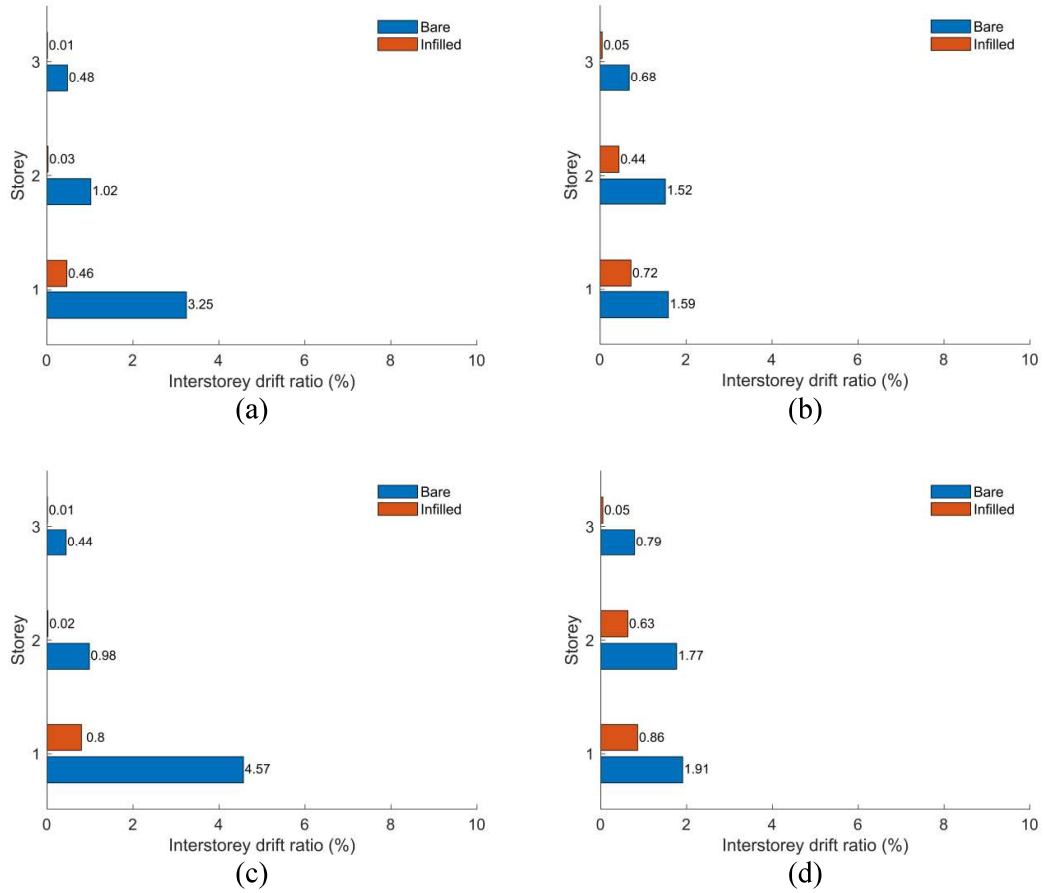

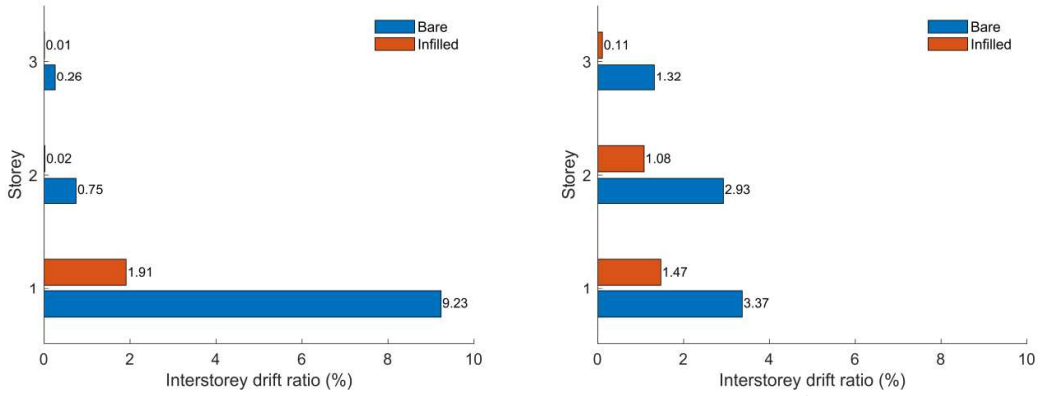

(e) (f)

Figure 8. Inter-storey drift in the X direction under positive modal load pattern for DL (a), SD (c) and NC (e) limit state, and inter-storey drift in the Y direction under negative uniform load pattern for DL (b), SD (d) and NC (f) limit state.

	Column rotation demand				**Panel zone Demand**	
	X		Y		Y	
	Bare	Infilled	Bare	Infilled	Bare	Infilled
DL	0.0339	0.0047	0.0203	0.0042	0.0197	0.0060
SD	0.0479	0.0082	0.0247	0.0059	0.0238	0.0083
NC	0.0972	0.0197	0.0447	0.0094	0.0426	0.0155

Table 7. Comparison of column rotation demand (rad) and panel zone distortion demand (rad) of the bare and the infilled frame.

In terms of local behaviour, Figure 8 shows the inter-storey drift at the CM of both the bare and the infilled frame, while Table 7 summarises the column rotation demand and panel zone distortion demand of the bare and the infilled frame. It is anticipated from Figure 8 that for the case study steel frame, the damage mainly develops on lower storey, which will experience larger drifts than higher storey. In particular, the presence of infills further concentrates the damage in the X direction onto the ground floor, which contributes to nearly 100% of the total lateral drift of the building. This indicates that the building possesses a weak column-strong beam (WCSB) feature, which is a common feature of existing steel buildings that were designed without sufficient ductility design and tend to cause larger

displacement at certain floors and higher seismic demand [44, 45]. In the case of the behaviour of structural components, the comparison of Table 7 concludes that the presence of infills dramatically reduces the local demand of columns and column panel zones for all limit states. This agrees with the findings in interstorey drift (Figure 8) that the infilled frame experience much smaller drifts at each limit state than the bare frame.

Furthermore, it is also essential to assess the behaviour of beams and columns in seismic performance of SMRFs with masonry infills. Only the results obtained with the 'modal' load pattern applied in the positive direction are presented hereafter for clarity. All beams and columns are checked for combined axial load and bending moment and combined shear and bending moment, following the design principle in EC3. The checks of beams and columns are carried out at the demand point of NC limit state in a similar manner as design to the ultimate limit state in EC3. Figure 9 and Figure 10 present the behaviour of the columns at the demand point of NC limit state. When the infills are not included, the ground floor columns are considered to be unsafe in X direction, as shown in Figure 9a and Figure 10a, where significant yielding due to bending is observed. However, when the infills are present, the columns are protected since the bending moment is reduced and the yielding on columns become less severe, even though a higher base shear is induced on the infilled frame at the NC limit state than on the bare frame. Similarly, Figure 9b and Figure 10b indicate that yielding of columns in the Y direction is also effectively prevented by the presence of infills. Figure 11 and Figure 12 present the behaviour of beams, which clearly show that in all cases the beams are within the safe range due to the WCSB feature of the case study building. Despite that, the effects of infills can still be observed, particularly in the X direction, where the infills tend to reduce the shear force and bending moment of beams but result in slightly higher axial force. The above observation suggests that the infills are able to protect the beams and columns of the case study building from significant yielding during strong

earthquakes, which explains why the case study building survived the 2016 Central Italy earthquakes. It also demonstrates the necessity of including infills in the numerical models for assessing existing buildings, as the model of bare frame provides estimates that are much conservative compared to the case of infilled frame and will lead to much more expensive retrofit solutions.

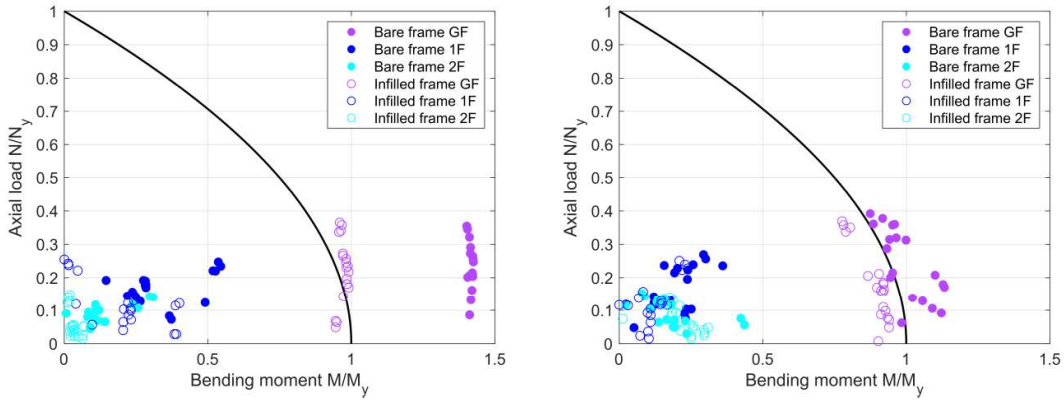

(a) (b)

Figure 9. Axial force-bending moment interaction of columns in the bare and infilled frame at the demand point of NC limit state: (a) in the longitudinal direction and (b) in the transverse direction.

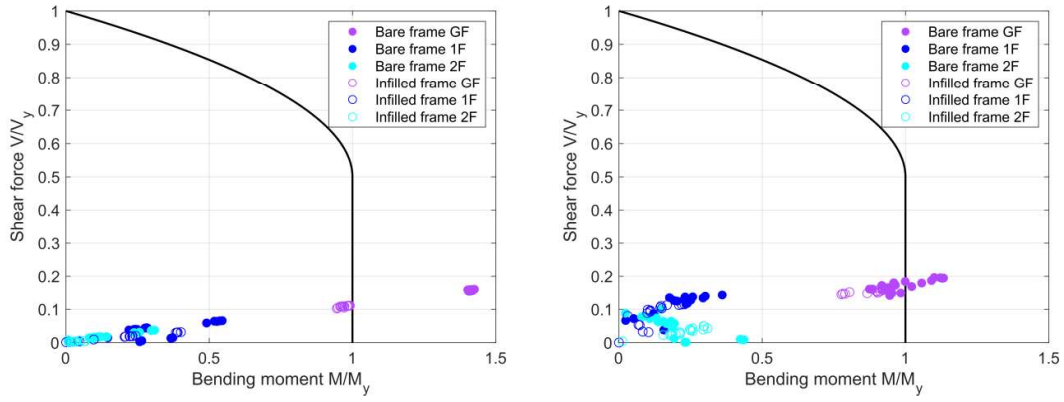

(a) (b)

Figure 10. Shear force-bending moment interaction of columns in the bare and infilled frame at the demand point of NC limit state: (a) in the longitudinal direction and (b) in the transverse direction.

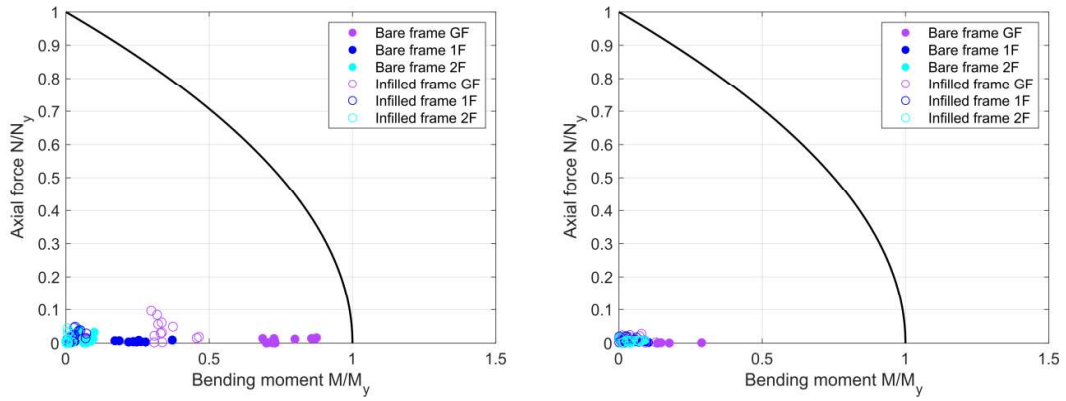

(a) (b)

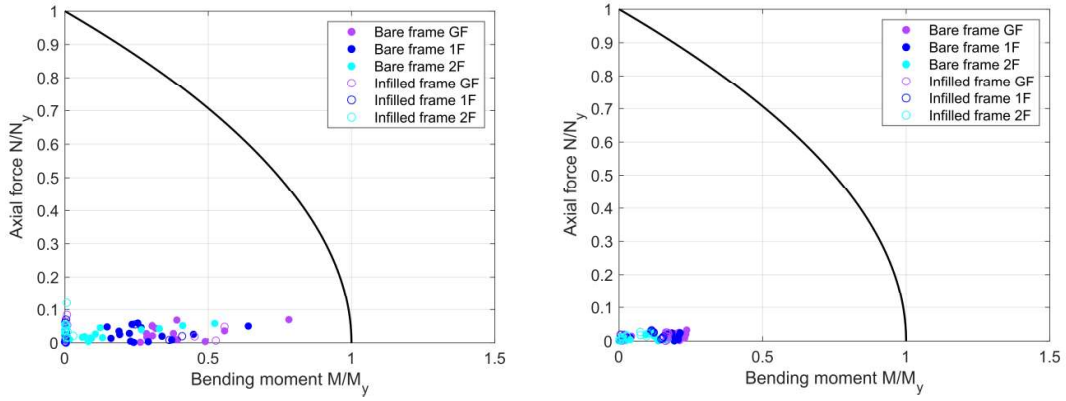

(c) (d)

Figure 11. Axial force-bending moment interaction of beams in the bare and infilled frame at the demand point of NC limit state in the longitudinal direction: (a) external beams, (b) internal beams, and in the transverse direction: (c) external beams, (d) internal beams.

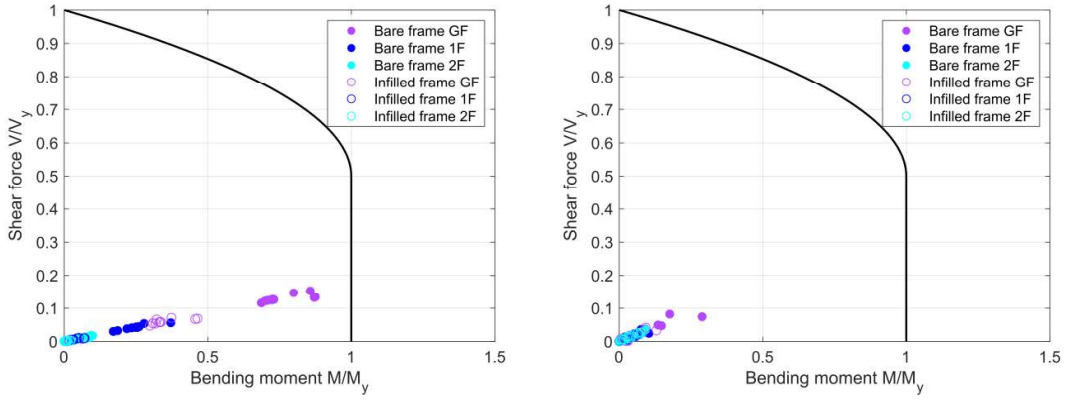

(a) (b)

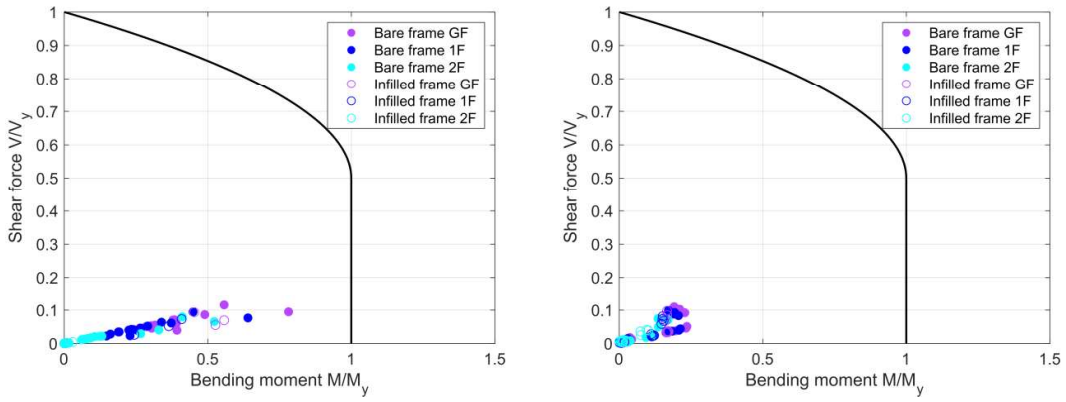

(c) (d)

Figure 12. Shear force-bending moment interaction of beams in the bare and infilled frame at the demand point of NC limit state in the longitudinal direction: (a) external beams, (b) internal beams, and in the transverse direction: (c) external beams, (d) internal beams.

Safety checks were carried out using the criteria proposed in Section 4. The chord yield rotation is, as suggested in ASCE41-17 [7], calculated using Eq.1 for beams and columns, since EC8-3 does not offer any proposal regarding the determination of yield rotations:

$$\theta_y = \frac{M_{pl,Rd}L}{6EI} \#\#\#\#\#(1)$$

where $M_{pl,Rd}$ is the plastic moment capacity, L is the length of element, E is the Young's modulus and I is the second moment of area. In this regard, the readers can also make reference to a recent project [46, 47] about the characterisation of steel components, which also developed expression of yield rotation of European steel beams and columns.

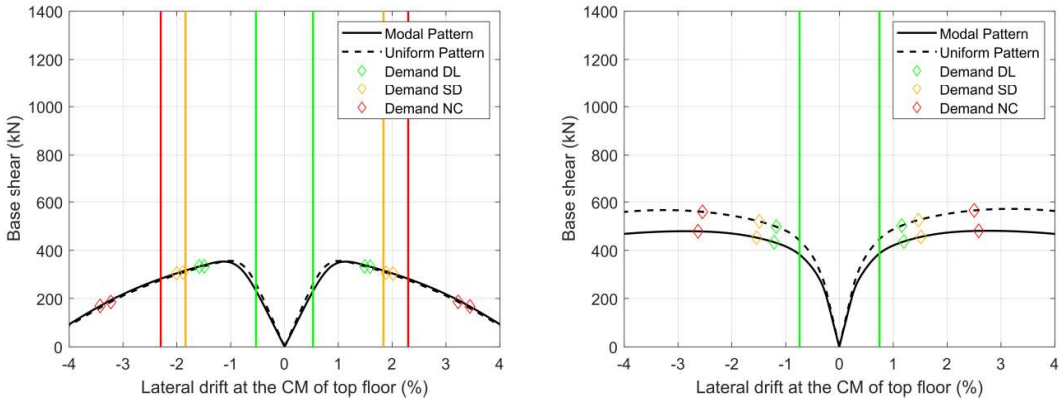

(a) (b)

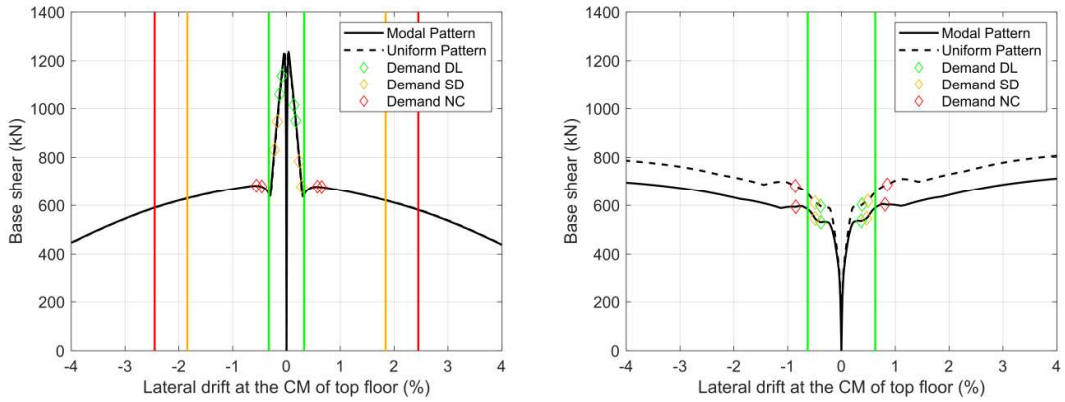

(c) (d)

Figure 13. Comparison of seismic demands and chord rotation capacities of the bare frame: (a) X direction and (b) Y direction; the infilled frame: (c) X direction and (d) Y direction.

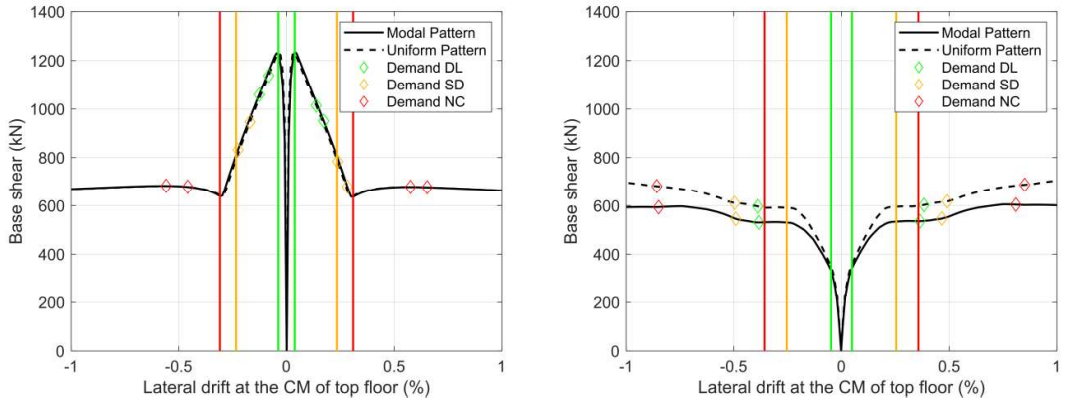

(a) (b)

Figure 14. Comparison of seismic demands and masonry infill capacities of the infilled frame: (a) X direction and (b) Y direction.

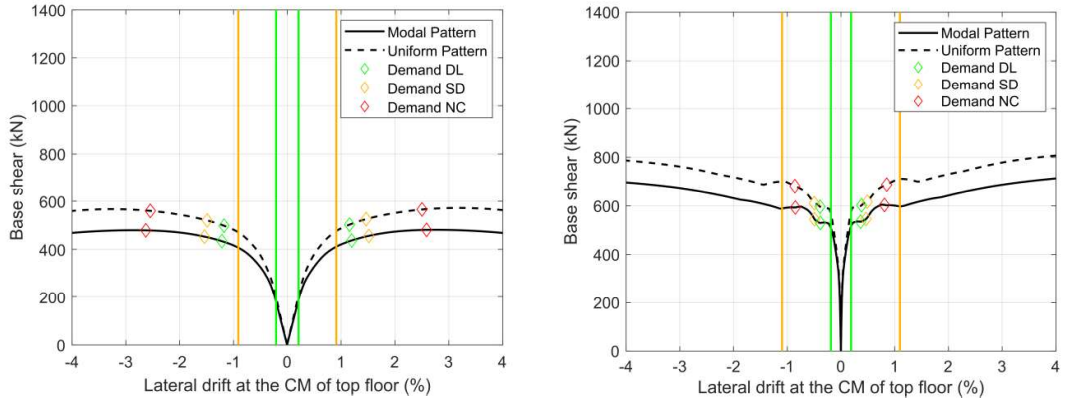

(a) (b)

Figure 15. Comparison of seismic demands and panel zone capacities: (a) the bare frame and (b) the infilled frame.

The comparison of demands and capacities are summarised from Figure 13 to Figure 15. The chord rotation capacities for SD and NC limit state in the Y direction are not presented indicate because they are related to a lateral drift larger than 5% of the total height of structure. Figure 13 shows that the infilled frame tends to reach chord rotation limits at smaller roof drift than the bare frame, especially in the longitudinal direction, where the contribution from infills are much more significant. This is because the presence of infills attracts much larger seismic loads, and once the infills loss their load carrying capacity, the seismic loads will be re-distributed to the structural components, in particular to columns in this case study, causing them to experience severe yielding at smaller drift of top floor than those in the bare frame. It is also found that the capacities of the case study building are controlled by either the behaviour of column panel zones or the interstorey drift limits if they are present, which demonstrates the potential inadequate of the chord rotation capacity in EC8-3 and the necessity of introducing criteria of additional parameters for the assessment of existing SMRFs. The safety checks demonstrate that, in terms of structural components, the bare frame fails all three limit states with the capacities being significantly lower than the demands, as shown in Figure 13ab and Figure 15a. However, for the infilled frame, the chord rotation (Figure 13cd) and the panel zone (Figure 15b) criteria show that only the DL limit state in the Y direction is slightly exceeded, which suggests that the case study building will experience yielding in columns and column panel zones, but the overall structure are not likely to collapse. Similarly, considering the limits of infills, Figure 14 shows that the infills in both X and Y direction will be severely damaged during strong earthquakes. In summary, the results of safety checks indicate that the infilled frame will experience significant damage on infill walls, however, global collapse of the steel structure will not happen, despite significant yielding may be found on steel components, especially at the beam-column

connections. This prediction of damage condition is believed to be similar to the real damage pattern surveyed on site as introduced in Section 5.1.

		d_y^* (cm)	d_u^* (cm)	μ	T_1* (sec)	q
X	Bare	7.21	9.99	1.39	1.89	1.39
	Infilled	0.16	0.54	3.38	0.15	1.48
Y	Bare	11.71	36.80	3.14	1.84	3.14
	Infilled	0.50	2.78	5.56	0.39	4.56

Table 8. Ductility (μ) and behaviour factor (q) of the bare and infilled frame (* represents the property of the equivalent SDOF system).

Finally, the reduction factor R, also known as the behaviour factor q in EC8, was determined based on the R-μ-T relationship in N2 method [25, 27] assuming zero overstrength, where μ and T are the global deformation ductility and first period of the equivalent SDOF system. μ is determined by taking the ratio of the maximum displacement d_u^*, which corresponds to the formation of plastic mechanism, and yield displacement d_y^* of the idealised curve of the SDOF system. In this case study, given the similarity between elastic perfectly plastic curves and elastic plastic curves with strain hardening, the R-μ-T relationship in [25] is adopted for all cases, excluding the cases of infilled frame in X direction for which the R-μ-T relationship in [27] is adopted. The results are summarised in Table 8. It is found that in this case study the values of q for the infilled frame are larger than those of the bare frame in both the X and Y direction. The smaller value of q from the X and Y direction, 1.39 for the bare frame and 1.48 for the infilled frame, is taken as the upper limit of q-factor to be used in assessment, regardless of the orientation of columns and significance of masonry infills. Compared to the value of 2 that is recommended in EC8-3, the use of code-recommended value will underestimate the seismic load and lead to unsafe retrofit design. However, considering the fact that EC8-3 does not recommend q-factor approach to be used in the assessment of

existing buildings, further investigations into appropriate values of q for existing steel buildings, with or without infills, should be carried out.

5.5 Verification of the proposed NSA procedure using non-linear dynamic analyses

This section contains the implementation of non-linear dynamic analysis (NDA) methods on the case study steel building under bi-directional earthquake loadings according to the provisions in EC8-3, whose results will be used to verify the reliability of the proposed pushover procedure. Two groups of ground motion records, namely Group A and B, were selected based on the target spectrum for SD limit state using the software REXEL [48], which is an effective tool for selecting earthquake records developed by the University of Naples Federico II. The earthquake records are provided by the Italian Accelerometric Archive of Waveforms [49] and the European Strong-Motion Data [52]. Group A contains seven bi-directional ground motion records, whose X-components achieve spectral compatibility to the target spectrum in the X direction. Similarly, Group B also contains seven bi-directional ground motion records but with their Y-components achieve compatibility to the target spectrum in the Y direction. The definition of compatibility here is based on the requirement in EC8-3, as introduced in Section 3. The purpose of selecting two groups of earthquake records is that when investigating the structural performance in one direction, the effects of the earthquake component in the other direction, for example, torsion, will be accounted for. In other words, Group A is aimed at obtaining the structural behaviour in X direction while Group B is aimed at the structural behaviour in Y direction. For the DL and NC limit state, the same records selected for SD limit state were scaled accordingly with scaling factors 0.79 and 1.71 to match the corresponding target spectrum. Figure 16 shows the response spectra of select records corresponding to 5% damping and their compatibility with the target spectrum of SD limit state. In order to perform the dynamic analysis, a

Rayleigh damping model is added to the structural model, where 5% damping is assigned to the first mode in the X and Y direction.

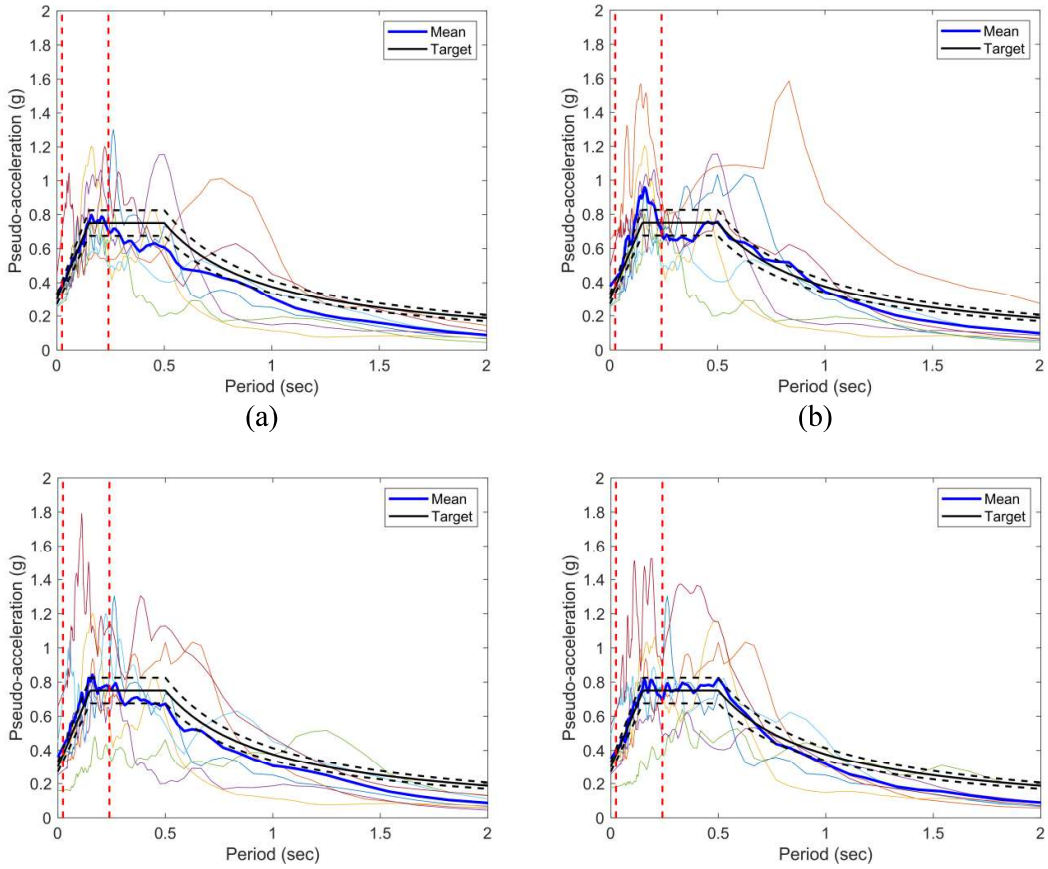

Figure 16. Mean spectrum of the X-spectrum compatible earthquake records: (a) in the X direction, (b) in the Y direction; and mean spectrum of the Y-spectrum compatible earthquake records: (c) in the X direction, (d) in the Y direction.

Table 9 summaries the target displacements for each limit state obtained as the mean value of the maximum response from each group, together with the estimates from previous NSA. Firstly, it is found that the proposed NSA procedure using the N2 method for infilled buildings systematically overestimates the roof drifts in the X direction, but the discrepancy is much smaller at the NC limit state than at the DL limit state. The same situation is observed in [27], where during the validation of the proposed R-μ-T relation for infilled buildings, it is found that smaller R, i.e. lower seismic loads, leads to relatively larger

558 discrepancy at short period (less than 0.5sec). However, in the Y direction, where a multi-
559 linear idealisation of capacity curves is utilised, good agreement between the estimates of
560 roof drifts from NDA and NSA is achieved. Also, the proposed NSA method is able to
561 achieve good estimates of roof deformation at higher seismic loads that are critical to the
562 collapse of existing buildings.

563 Apart from the global deformation, the estimated local deformation, e.g. rotation of beams
564 and columns, distortion of panel zones and infill drifts, are also compared to assess the
565 reliability of the proposed NSA method. Figure 17 presents the comparison of inter-storey
566 drifts obtained from the proposed NSA and the code-based NDA. The results are concluded
567 to be in consistency with the roof deformation. It is found that at the NC limit state, the NSA
568 may underestimate the local demands, such as the interstorey drift in Y direction in Figure
569 17f, column rotation in X direction in Figure 20e and infill drift in Figure 22ef, if the results
570 from the code-based NDA are considered as the 'exact' response. Despite this, in most cases,
571 the NSA provides slightly conservative estimates of seismic demands, especially for those
572 critical components, such as the columns and panel zones in this case. Considering the
573 simplicity of NSA and the inherent uncertainties in the code-based NDA, this discrepancy is
574 believed to be acceptable.

		DL		SD		NC	
	Group	X	Y	X	Y	X	Y
NDA	A	0.05	0.38	0.18	0.48	0.62	0.97
	B	0.08	0.35	0.18	0.45	0.46	0.89
NSA		0.17	0.40	0.28	0.51	0.65	0.89

575 Table 9. Mean value of maximum roof drifts (%) obtained from Group A and B ground
576 motion records.

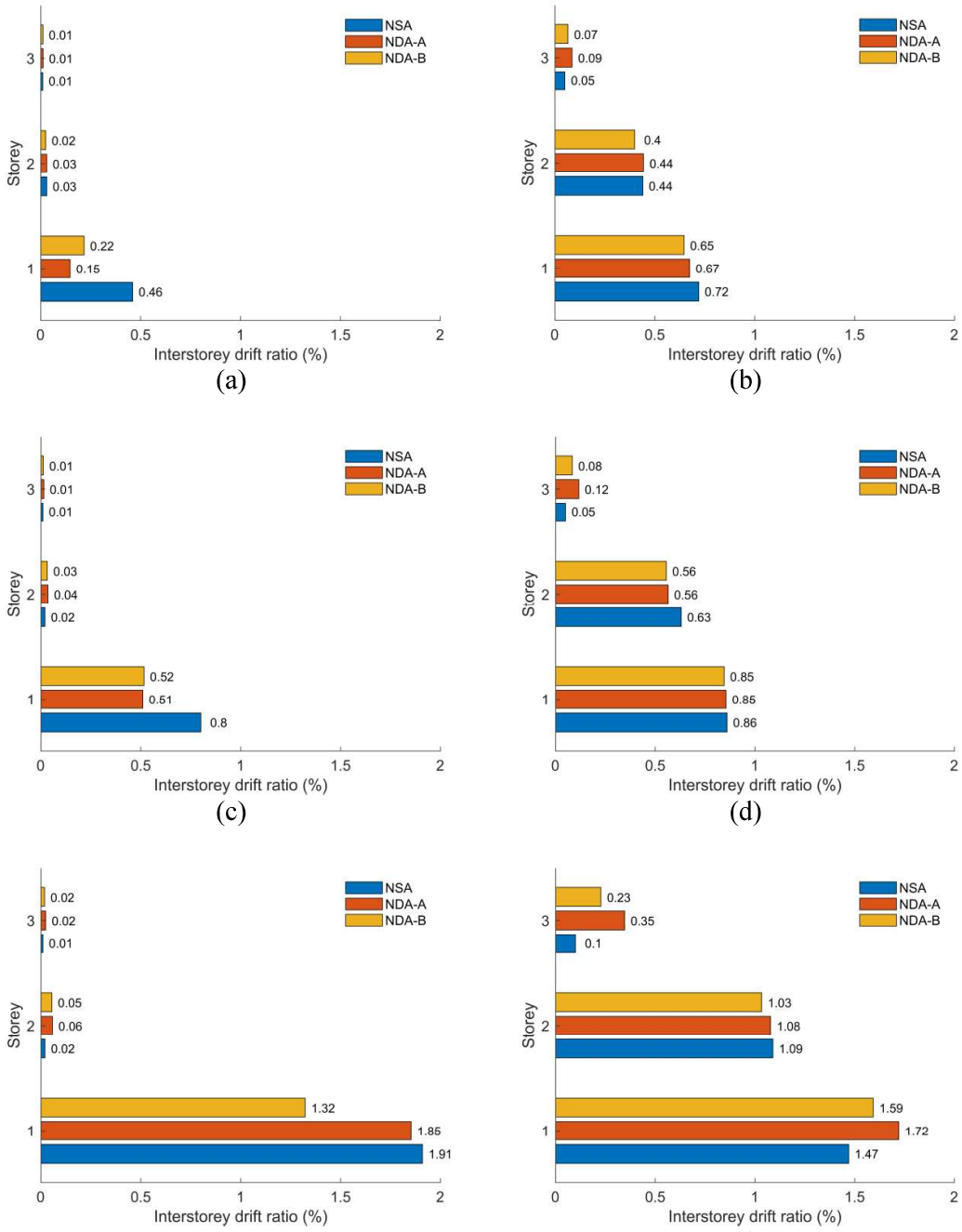

Figure 17. Comparison of inter-storey drift in the X direction for DL (a), SD (c) and NC (e) limit state, and in the Y direction for DL (b), SD (d) and NC (f) limit state.

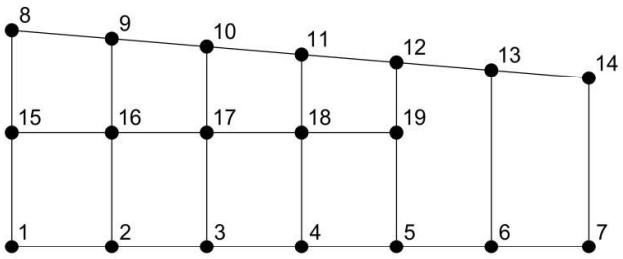

Labelling of columns and panel zones

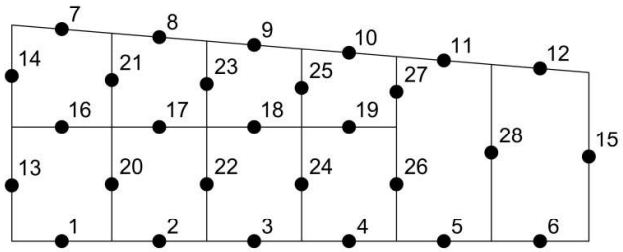

Labelling of beams and infill panels (perimeter only)

585
586 Figure 18. Labelling of columns, panel zones, beams and infill panels for interpretation of
587 Figure 20 to 23.

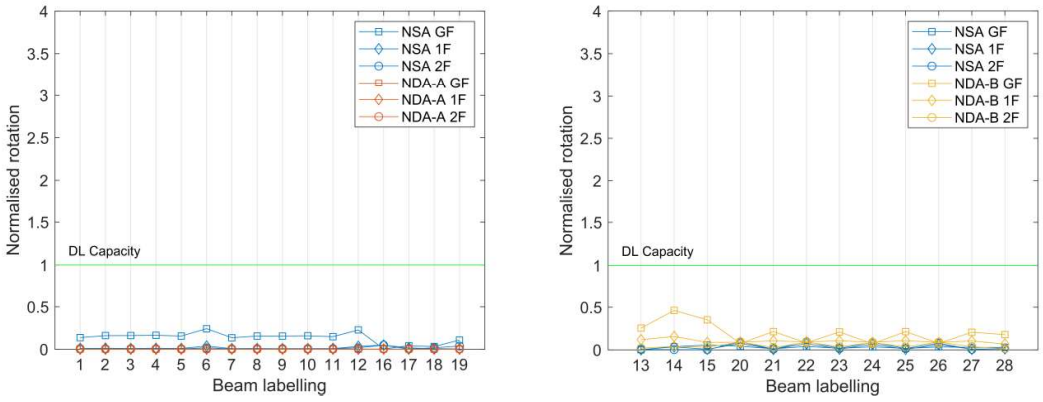

588
589 (a) (b)

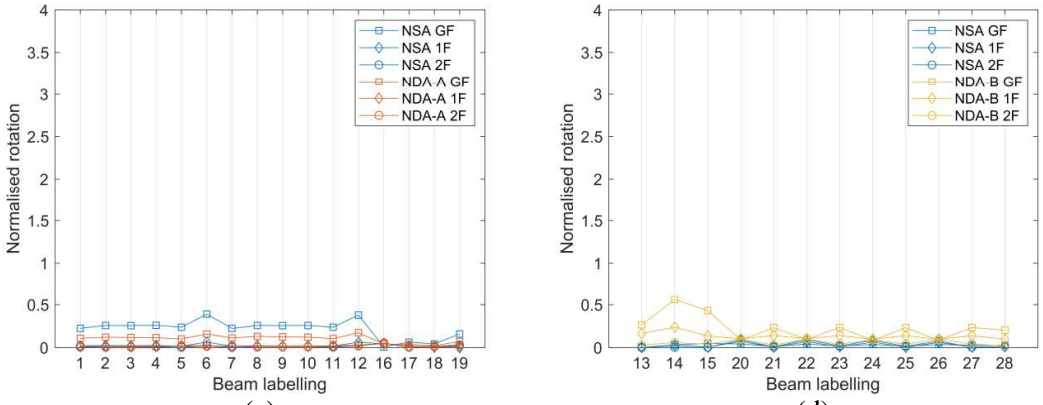

590
591 (c) (d)

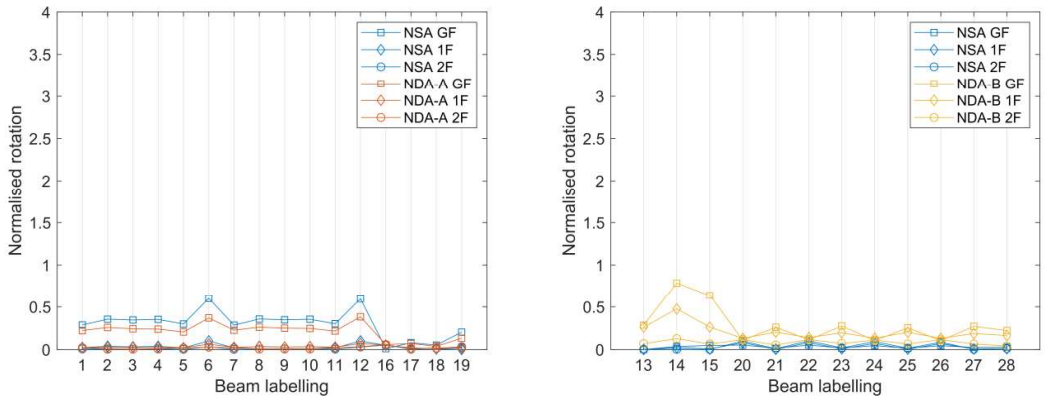

(e) (f)

Figure 19. Comparison of beam rotation demands in the X direction for (a) DL, (c) SD and (e) NC limit state, and in the Y direction for (b) DL, (d) SD and (f) NC limit state.

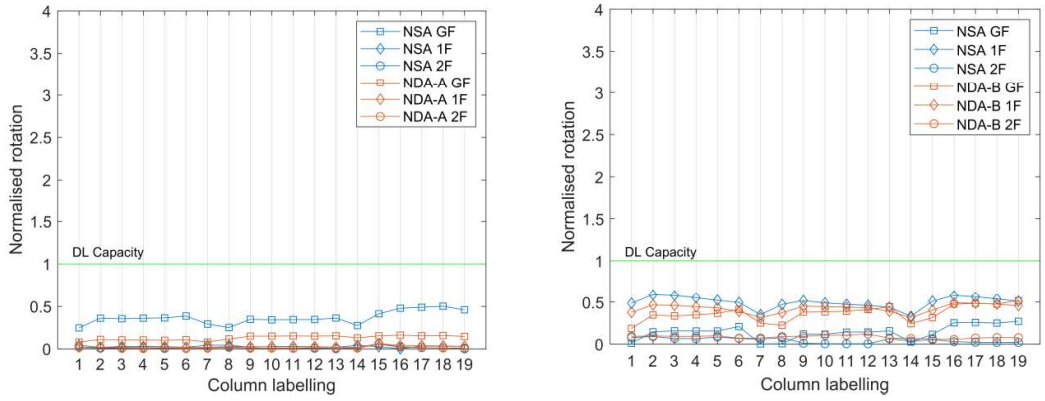

(a) (b)

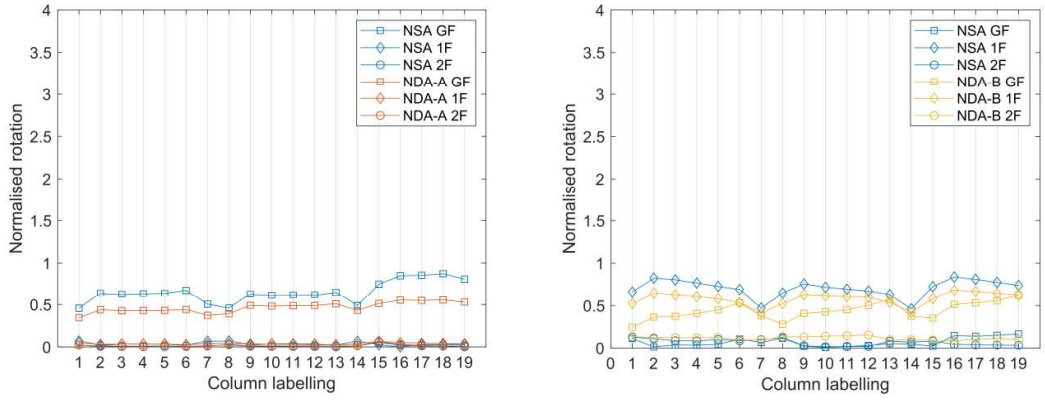

(c) (d)

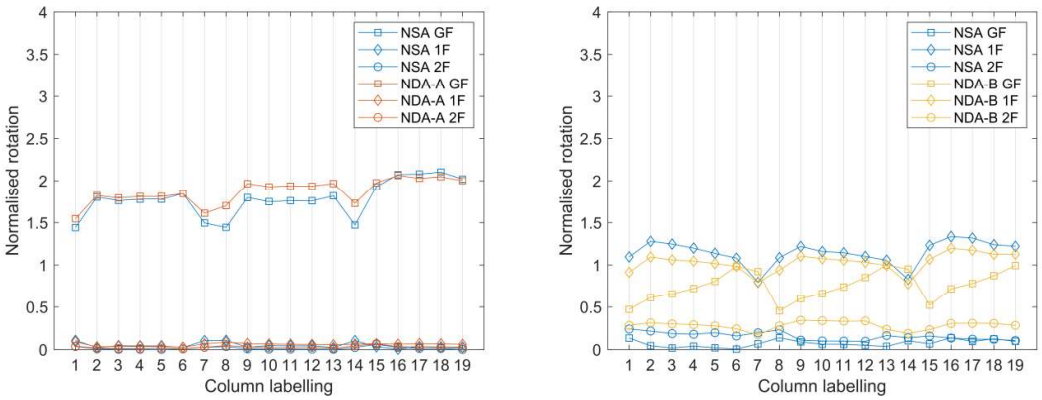

(e) (f)

Figure 20. Comparison of column rotation demands in the X direction for (a) DL, (c) SD and (e) NC limit state, and in the Y direction for (b) DL, (d) SD and (f) NC limit state.

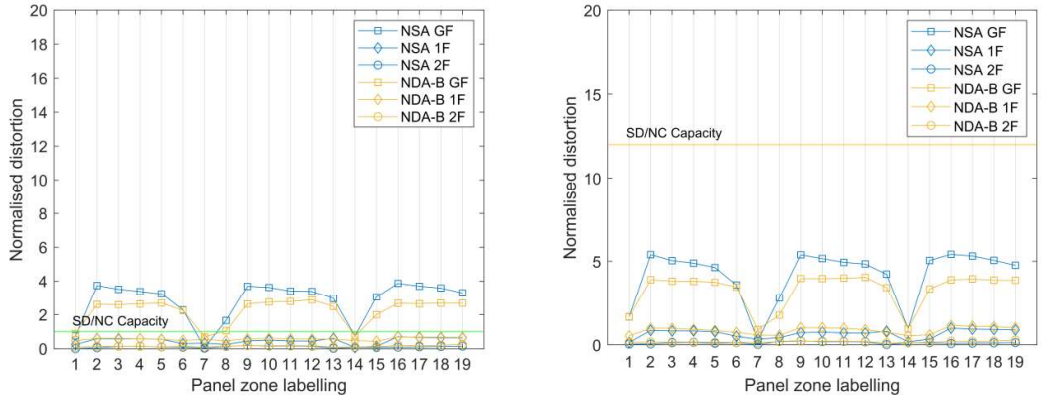

(a) (b)

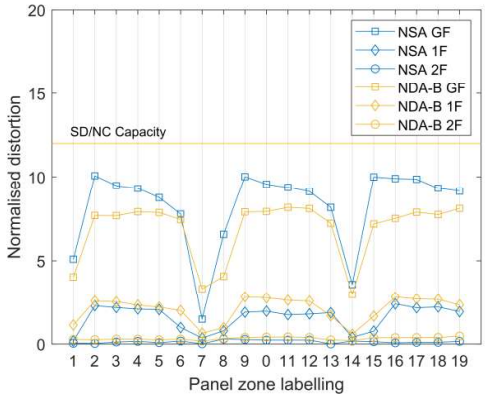

(c)

Figure 21. Comparison of panel zone distortion demands in the Y direction for (a) DL, (b) SD and (c) NC limit state.

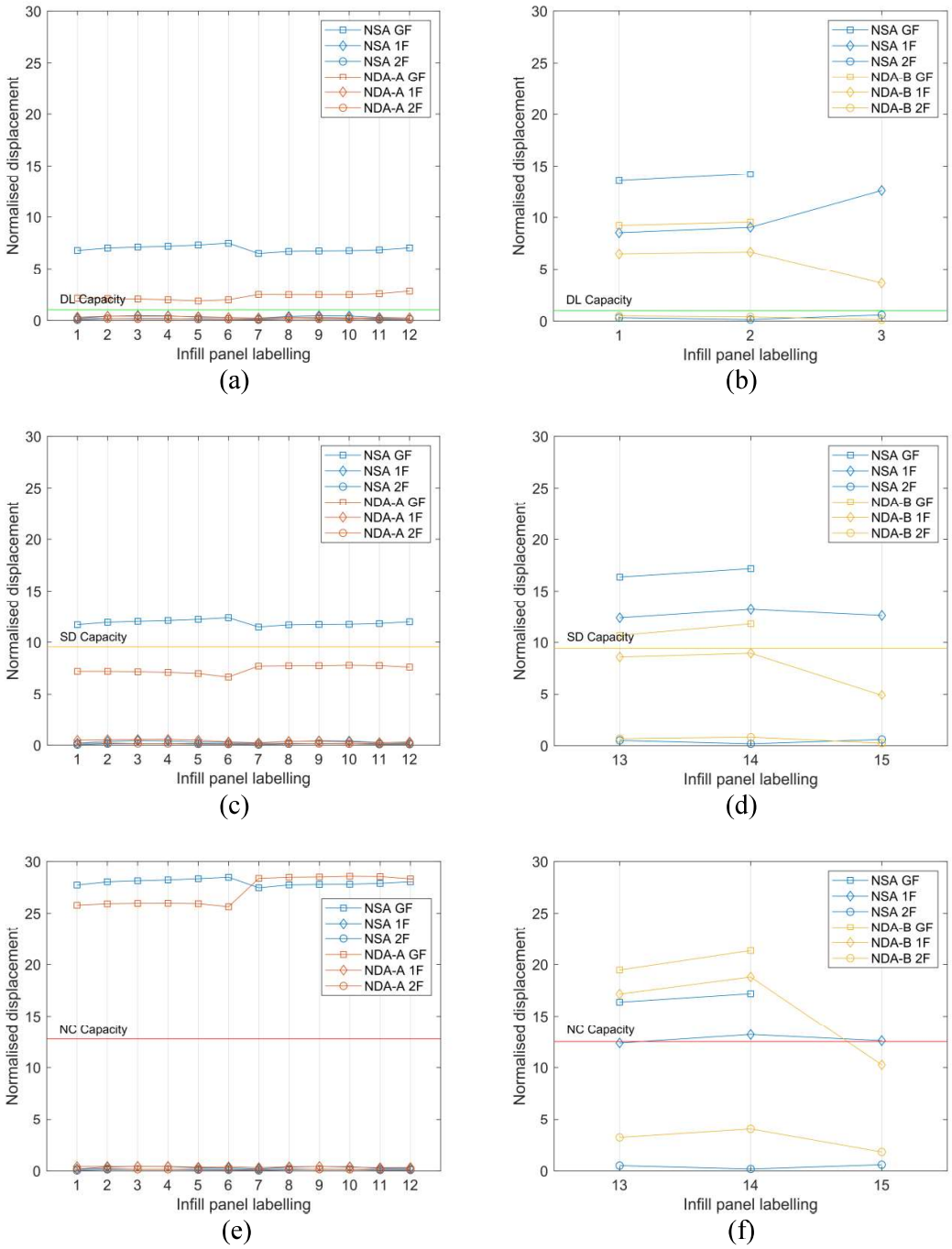

Figure 22. Comparison of in-plane masonry infill drift demands in the X direction for (a) DL, (c) SD and (e) NC limit state, and in the Y direction for (b) DL, (d) SD and (f) NC limit state.

5.6 Fragility analysis

In the final section, fragility analysis was carried out on the bare and infilled frame to compare the behaviour of both frames in a probabilistic manner. A suite of ten ground motion

621 records at Amatrice was selected on Italian Accelerometric Archive of Waveforms [49],
622 whose information is summarised in Table 10. The intensity measure (IM) was chosen to be
623 the 5% damping spectral acceleration at the fundamental period of the bare frame in the
624 longitudinal direction. Meanwhile, the engineering demand parameter (EDP) was chosen to
625 be the column rotation in X direction and panel zone distortion in Y direction. This choice
626 was made based on the previous assessment results that the overall structural safety is
627 controlled by the column rotation and panel zone distortion in the X and Y direction,
628 respectively.

Event	**M_L**	**Epicentre (km)**	**$S_{a,x}(T_1)$ (m/s²)**		**$S_{a,y}(T_1)$ (m/s²)**	
			Bare	Infill	Bare	Infill
1	6.0	8.5	1.45	5.35	1.19	18.53
2	6.1	26.4	0.87	6.85	1.53	9.96
3	5.4	9.7	0.32	5.89	0.29	1.70
4	4.7	3.1	0.13	6.59	0.14	1.95
5	5.4	11.3	0.56	4.24	0.39	5.82
6	4.3	3.6	0.09	4.23	0.14	2.47
7	4.5	3.6	0.11	2.03	0.16	3.33
8	4.3	3.6	0.09	2.90	0.06	1.28
9	5.3	14.4	0.23	1.53	0.32	4.58
10	5.4	20.9	0.25	1.49	0.19	1.61

629 Table 10. Summary of selected ground motion records.

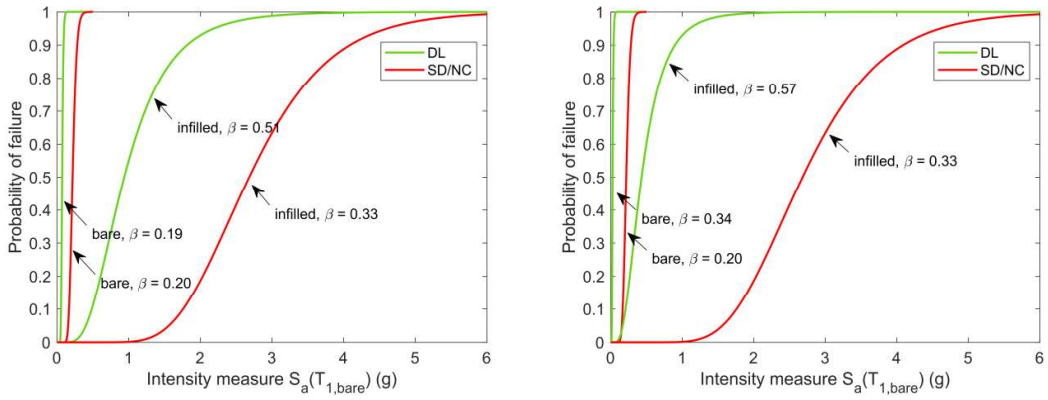

(a) (a)

Figure 23. Fragility curves of the case study frame in (a) X direction controlled by column rotation limits and (b) Y direction controlled by panel zone limits.

Figure 23 shows the fragility curves obtained for the bare and infilled frame. It is evident that the infilled frame possesses a much larger lateral strength than the bare frame. The exceedance of DL and SD/NC limit state of the bare frame happens mainly around 0.1 and 0.3g, respectively. The presence of infills complicates the seismic performance of steel frames, making it more sensitive to different ground motions and leading to a larger discrepancy as shown in Figure 23. Despite that, it is still obvious that the exceedance of DL and SD/NC limit state of the infilled frame tends to take places at a much higher intensity level, with median being about 0.9 and 2.7g respectively for DL and SD/NC limit state in the X direction and 0.5 and 2.7g in the Y direction.

Furthermore, it is found that the fragility curves of both the bare and infilled frame in the X direction for SD/NC limit state are identical to those in the Y direction. This is because that in all cases the failure of structures occurred due to instability before the chosen limit state was reached, i.e. the structure failed due to global instability before the columns and panel zones reach their capacities for SD and NC limit state. This also explains why the curve for SD limit state in the X direction is identical to the one for NC limit state, hence two fragility curves corresponding to three different criteria defined. The failure of columns to sufficiently develop their ductility both in terms of chord rotation and panel zone distortion suggests that

651 the case study building is very vulnerable to large horizontal excitations, which reveals the
652 fact that as a typical existing steel building it was not adequately designed for seismic loading
653 and with critical P-Δ issues. This observation also indicates a major drawback of the propose
654 assessment procedure which lacks appropriate criteria to account for the instability issue,
655 since it may be more critical in some cases to define the failure of structures.

656 **6 Conclusions**

657 In this paper, an improved non-linear procedure of assessing existing SMRFs is proposed and
658 its application on a case study steel building is presented. The proposed procedure addressed
659 some of the issues in the current EC8-3, such as its limited application to SMRFs with infills
660 and lack of criteria for column panel zones. Refined 3D models of the steel building were
661 developed in OpenSees, which includes the modelling of masonry infill walls and column
662 panel zones in addition to the basic bare frame. The effects of masonry infills on the response
663 of beams and columns were also investigated in this paper.

664 Modal analyses were performed first to found out the effects of different modelling
665 parameters on the modal properties of the case study building. It is found that the presence of
666 infills reduced the fundamental periods of the case study frame by over 90% in the X
667 direction and by over 70% in the Y direction. Such huge reduction in fundamental periods
668 noticed in this case study may not be appropriate for all existing buildings, yet it still
669 confirms the fact that the infills contribute to the lateral stiffness of existing steel frames at a
670 much higher degree than to modern steel frames, since existing steel frames tend to be more
671 flexible than modern steel frames. On the other hand, the inclusion of column panel zones
672 slightly increased the fundamental period in the Y direction by about 10%.

673 The results of NSA demonstrate the effects of masonry infills on the overall structural
674 behaviour and response of beams and columns. The infills significantly increased the lateral

675 stiffness and strength of the case study building, reducing the demand of roof displacement
676 by around 85% in the X direction and 70% in the Y direction. The case study building was
677 also found to possess the feature of WCSB and the infills concentrated the damage to lower
678 floors of the building, particularly in the X direction where the lateral drift of ground floor
679 accounts for nearly 100% of total drift at roof level. Besides, at the demand point of NC limit
680 state, the columns in the bare frames have significantly yielded and were unsafe considering
681 both the interaction between axial load and bending moment, and the interaction between
682 shear force and bending moment, while those in the infilled frame were still safe and only
683 slightly yielded. This observation suggests that the masonry infill are likely to protect the
684 building during strong earthquakes, as long as they are not completed failed and loss all their
685 loading carrying capacities, especially those on lower floors.

686 Lastly, code-based NDA was performed to verify the reliability of the proposed NSA
687 procedure. It is found that the NSA tends to provided slightly conservative estimates of
688 global and local demands, although in some cases for the NC limit state, the NSA
689 underestimates the demands, if compared to the results from NDA. The results of safety
690 verification generally well match the results obtained from NSA. However, a major drawback
691 of the proposed assessment procedure was found through a preliminary fragility analysis,
692 which indicates that appropriate criteria that account for structural instability should be
693 included in the future as the P-Δ effect may prevent the structural components from
694 sufficiently developing their ductility. In summary, considering the simplicity and efficiency
695 of the proposed NSA compared to code-based NDA, the proposed NSA provides acceptable
696 assessment results of the case study building.

697 Another essential aspect in the field of assessing existing buildings that is not accounted for
698 in the proposed NSA method is the soil-structure interaction, which also have non-negligible
699 impact on the modal properties of steel frames, hence their seismic performance. Specific

700 requirements on such aspect are not included in the current EC8-3, either. Therefore, possible
701 solutions to account for the effects of soil-structure interaction, such as improving the
702 numerical model or modifying the natural periods and corresponding mode shapes, should be
703 investigated in the future.

704 **7 Acknowledgement**

705 The financial support from Seismic Engineering Research Infrastructure for HITFRAMES
706 (SERA) Project, funded within the H2020-INFRAIA-2016-2017 Framework Program of the
707 European Commission under grant agreement No.730900 is greatly appreciated. Any
708 opinions, findings and conclusions, or recommendations expressed in this paper are those of
709 the authors and do not necessarily reflect those of SERA sponsors.

References

1. Di Sarno L, Elnashai AS, Bracing systems for seismic retrofitting of steel frames, *Journal of Constructional Steel Research*, 2009; 65(2):452-465.
2. Gupta A, Krawinkler H, *Seismic Demands for the Performance Evaluation of Steel Moment Resisting Frame Structures*, Ph.D. Thesis, Stanford University, 1999.
3. Di Sarno L, Paolacci F, Sextos AG, Seismic performance assessment of existing steel buildings: a case study, *Key Engineering Materials,* 2018; 763:1067-1076.
4. Li Q, Ellingwood BR, Damage inspection and vulnerability analysis of existing buildings with steel moment-resisting frames, *Engineering Structures,* 2008; 30(2):338-351.
5. Güneyisi EM, Seismic reliability of steel moment resisting framed buildings retrofitted with buckling restrained braces, *Earthquake Engineering & Structural Dynamics,* 2012; 41(5):853-874.
6. British Standard Institution, BS EN 1998-3:2005, Eurocode 8. Design of structures for earthquake resistance – Part 3: Assessment and retrofitting of buildings, London: 2005.
7. American Society of Civil Engineering, ASCE41-17, Seismic evaluation and retrofit of existing buildings, Reston, Virginia: 2017.
8. SEAOC, Vision 2000: performance-based seismic engineering of buildings, California: 1995.
9. Applied Technology Council, FEMA 273, Guidelines for the seismic rehabilitation of buildings, Washington, D.C.: 1997.
10. American Society of Civil Engineering, FEMA 356, Prestandard and commentary for the seismic rehabilitation of buildings, Washington, D.C.: 2000.

11. Araújo M, Castro JM, A critical review of European and American provisions for the seismic assessment of existing steel moment-resisting frame buildings, *Journal of Earthquake Engineering*, 2018; 22(8):1336-64.

12. Mpampatsikos V, Nascimbene R, Petrini L, A critical review of the RC frame existing building assessment procedure according to Eurocode 8 and Italian seismic code. *Journal of Earthquake Engineering*, 2008; 12(S1):52-82.

13. Pinto PE, Franchin P, Assessing existing buildings with Eurocode 8 part 3: a discussion with some proposals, *InBackground documents for the "Eurocodes: background and applications" workshop*, Brussels, Belgium: 2008.

14. American Society of Civil Engineering, ASCE41-06, Seismic rehabilitation of existing buildings, Reston, Virginia: 2007.

15. American Society of Civil Engineering, ASCE41-13, Seismic evaluation and retrofit of existing buildings, Reston, Virginia: 2014.

16. Formisano A, Gamardella F, Mazzolani FM, Capacity and demand of ductility for shear connections in steel MRF structures, *Civil-Comp Proceedings,* 2013; 102.

17. Elghazouli, AY, Assessment of European seismic design procedures for steel frames structures, *Bulletin of Earthquake Engineering,* 2010; 8(1): 65-89.

18. Braconi A, Caprili S, Degee H, Guendel M, Hjiaj M, Hoffmeister B, Karamanos SA, Rinaldi V, Salvatore W, Somja H, Efficiency of Eurocode 8 design rules for steel and steel-concrete composite structures, *Journal of constructional steel research,* 2015; 112:108-129.

19. British Standard Institution, BS EN 1998-1:2005, Eurocode 8. Design of structures for earthquake resistance – Part 1: General rules, seismic actions and rules for buildings, London: 2004.

20. Fardis MN and Panagiotakos TB, Seismic Design and Response of Bare and Masonry-Infilled Reinforced Concrete Buildings Part II: Infilled Structures, *Journal of Earthquake Engineering,* 1997; 1(03): 475-503.

21. Asteris PG, Antoniou ST, Sophianopoulos DS and Chrysostomou CZ, Mathematical Macromodeling of Infilled Frames: State of the Art, *Journal of Structural Engineering*, 2011; 137(12): 1508-1517.

22. Smith BS, Methods for Predicting the Lateral Stiffness and Strength of Multi-Storey Infilled Frames, *Building Science*, 1967; 2(3):247-257.

23. Krawinkler H, Bertero VV and Popov EP, Inelastic Behaviour of Steel Beam-to-Column Subassemblages. *Report No. EERC 71-07*, Earthquake Engineering Research Center (EERC), University of California at Berkeley, 1971.

24. Castro JM, Elghazouli AY and Izzuddin BA, Modelling of the Panel Zone in Steel and Composite Moment Frames, *Engineering Structures*, 2004; 27(1):129-144.

25. Fajfar P, A nonlinear analysis method for performance-based seismic design. *Earthquake spectra*, 2000; 16(3):573-592.

26. Dolšek M, Fajfar P, The effect of masonry infills on the seismic response of a four storey reinforced concrete frame - a deterministic assessment, *Engineering Structures,* 2008; 30(11):3186-92.

27. Dolšek M, Fajfar P, Inelastic spectra for infilled reinforced concrete frames, *Earthquake engineering & structural dynamics*, 2004; 33(15):1395-1416.

28. Dolšek M, Fajfar P, Simplified Non-linear Seismic Analysis of Infilled Reinforced Concrete Frames, *Earthquake Engineering & Structural Dynamics*, 2005; 34(1):49-66.

29. Sextos AG, Katsanos EI, Manolis GD, EC8-based earthquake record selection procedure evaluation: Validation study based on observed damage of an irregular R/C building, *Soil Dynamics and Earthquake Engineering*, 2011; 31(4):583-597.

30. Katsanos EI, Sextos AG, Manolis GD, Selection of earthquake ground motion records: A state-of-the-art review from a structural engineering perspective, *Soil Dynamics and Earthquake Engineering*, 2010; 30(4):157-169.

31. Bradley BA, Design seismic demands from seismic response analyses: a probability-based approach, *Earthquake Spectra*, 2011; 27:213-224.

32. Li Q, Ellingwood BR, Performance evaluation and damage assessment of steel frame buildings under main shock–aftershock earthquake sequences. *Earthquake engineering & structural dynamics*. 2007; 36(3):405-27.

33. Di Sarno L, Amiri S. Period elongation of deteriorating structures under mainshock-aftershock sequences, *Engineering Structures*, 2019; 196:109341.

34. Di Sarno, L, Effects of multiple earthquakes on inelastic structural response, *Engineering Structures*, 2013; 56:673-681.

35. Antoniou S, Pinho R. Development and verification of a displacement-based adaptive pushover procedure, *Journal of earthquake engineering*, 2004; 8(05):643-661.

36. Elnashai AS. Advanced inelastic static (pushover) analysis for earthquake applications, *Structural engineering and mechanics*, 200; 12(1):51-70.

37. Chopra AK, Goel RK. A modal pushover analysis procedure for estimating seismic demands for buildings, *Earthquake engineering & structural dynamics*, 2002; 31(3):561-582.

38. Mazzoni S, McKenna F, Scott MH, Fenves GL, OpenSees command manual, *Pacific Earthquake Engineering Research (PEER) Centre*, 2006; 264.

39. Filippou FC, Popov EP, Bertero VV, Effects of Bond Deterioration on Hysteretic Behavior of Reinforced Concrete Joints, *Report EERC 83-19*, Earthquake Engineering Research Center, University of California, Berkeley: 1983.

40. Menegotto M, Pinto P, Method of Analysis for Cyclically Loaded Reinforced Concrete Plane Frames Including Changes in Geometryand Non-elastic Behavior of Elements Under Combined Normal Force and Bending, *Proceedings of IABSE Sympoium on Resistance and Ultimate Deformability of Structures Acted on by Well-Defined Repeated Loads, International Assoc. of Bridge and Structural Engineering*, 1973; 13:15-22.

41. Noh NM, Liberatore L, Mollaioli F, Tesfamariam S, Modelling of Masonry Infilled RC Frames Subjected to Cyclic Loads: State of the Art Review and Modelling with OpenSees, *Engineering Structures*, 2018; 150:599-621.

42. Smith BS, Methods for Predicting the Lateral Stiffness and Strength of Multi-Storey Infilled Frames, *Building Science*, 1967; 2(3):247-257.

43. Liberatore L, Decanini LD, Effect of Infills on the Seismic Response of High-Rise RC Buildings Designed as Bare According to Eurocode 8, *Ingegneria Sismica*, 2011; 3:7-23.

44. Roeder CW, Schneider SP, Carpenter JE, Seismic behavior of moment-resisting steel frames: analytical study, *Journal of Structural Engineering*, 1993; 119(6):1866-84.

45. Schneider SP, Roeder CW, Carpenter JE, Seismic behavior of moment-resisting steel frames: Experimental study, *Journal of Structural Engineering*, 1993; 119(6):1885-902.

46. Della Corte G, Terranciano G, Di Lorenzo G, Landolfo R, Characterising bolted end-plate beam-column joints using the component method, chapter 5. In: Sullivan TJ,

823 O'Reilly GJ (eds) Characterising the seismic behaviour of steel beam-column joints for
824 seismic design. Research report EUCENTRE 2014/01. IUSS Press, Pavia, Italy, 2014.

825 47. Roldán R, Sullivan TJ, Della Corte G. Displacement-based design of steel moment
826 resisting frames with partially-restrained beam-to-column joints, *Bulletin of Earthquake*
827 *Engineering*, 2016; 14(4):1017-1046.

828 48. Iervolino I, Galasso C, Cosenza E, REXEL: computer aided record selection for code-
829 based seismic structural analysis. *Bulletin of Earthquake Engineering*, 2010; 8: 339-362.

830 49. Working Group ITACA, Database of the Italian strong motion data, 2008.

831 50. Solomos G, Pinto A, Dimova S. A review of the seismic hazard zonation in national
832 building codes in the context of eurocode 8, *JRC Scientific and Technical Reports*, 2008.

833 51. Krawinkler H, Seneviratna GD. Pros and cons of a pushover analysis of seismic
834 performance evaluation, *Engineering structures*, 1998; 20(4-6):452-464.

835 52. Ambraseys, N, Smit, P, Sigbjornsson, R, Suhadolc, P and Margaris, B, Internet-Site for
836 European Strong-Motion Data, European Commission, Research-Directorate General,
837 Environment and Climate Programme, 2002.

838 53. Beiraghi H, Fundamental period of masonry infilled moment‐resisting steel frame
839 buildings, *The Structural Design of Tall and Special Buildings*, 2017; 26(5):1342.

UNIVERSITY OF LIVERPOOL

Dr. Luigi di Sarno
Senior Lecturer in Structural Design
Department of Civil Engineering &
Industrial Design
School of Engineering
University of Liverpool
Brodie Tower, Room 610
Liverpool L69 3GQ - UK
☎ Off: +44(0)151 794 3051
email.: luigi.di-sarno@liv.ac.uk

Liverpool, 24th February 2020

Dear Editor of Journal of Constructional Steel Research

I am writing to you to re-submit the revised version of the following joint technical paper:

"Seismic assessment of existing steel frames with masonry infills"

which discuss the numerical results of comprehensive inelastic analyses that were carried out for typical existing steel frames which are built without seismic details.

The paper does not contain any conflict of interests.

Yours Sincerely,

Dr. Luigi di Sarno